Cortico-thalamo-cortical interactions modulate electrically evoked EEG responses in mice

AUTHORS

Leslie D. Claar[1,2,3,*], Irene Rembado[1,2,*], Jacqulyn R. Kuyat[1], Lydia C. Marks[1], Shawn R. Olsen[1], Christof Koch[1,*]

[1] MindScope Program, Allen Institute, Seattle, United States

[2] These authors contributed equally to this work.

[3] Lead Contact

* Correspondence: lesliec@alleninstitute.org, irene.rembado@alleninstitute.org, christofk@alleninstitute.org

SUMMARY

Perturbational complexity analysis predicts the presence of human consciousness by stimulating the brain with brief pulses, recording electroencephalography (**EEG**) responses, and computing their spatiotemporal complexity. We examined the underlying neural circuits in mice by directly stimulating cortex while recording with EEG and Neuropixels probes during wakefulness and isoflurane anesthesia. When mice are awake, stimulation of deep cortical layers reliably evokes locally a brief pulse of excitation, followed by a bi-phasic sequence of 120 ms profound *off* period and a *rebound* excitation. A similar pattern, partially attributed to burst spiking, is seen in thalamic nuclei, and is associated with a pronounced late component in the evoked EEG. We infer that cortico-thalamo-cortical interactions drive the long-lasting evoked EEG signals elicited by deep cortical stimulation during the awake state. The cortical and thalamic off period and rebound excitation, and the late component in the EEG, are reduced during running and absent during anesthesia.

Key words: EEG, perturbational complexity, electrophysiology, anesthesia, thalamic burst, cortico-thalamo-cortical

INTRODUCTION

A long-standing clinical challenge has been to discover sensitive and specific biomarkers of consciousness. One obvious candidate is electroencephalography (**EEG**), with high amplitude delta activity usually taken as an indicator of absence of consciousness, as during deep sleep, anesthesia, in vegetative state patients (also known as behavioral unresponsive wakefulness syndrome), or in coma (Bai et al., 2017; Kobylarz & Schiff, 2005; Schiff et al., 2014). However, given the vast diversity of patients and their etiology, spontaneous EEG can show very unusual spatio-temporal patterns, with attendant high false alarm and miss rates in diagnosing individual patients with disorders of consciousness (Farisco et al., 2022; Frohlich et al., 2021; Thibaut et al., 2019). More promising is the perturbational EEG (Bai et al., 2021), in which the brain is probed by a brief magnetic pulse (generated via transcranial magnetic stimulation, **TMS**, applied to the skull) and the resulting cortical activity is recorded using a high-density EEG electrode array (Casali et al., 2013; Casarotto et al., 2016; Massimini et al., 2005; Rosanova et al.,

2018). A simple algorithm then computes the *perturbational complexity index* (**PCI**) of the brain's reverberations to this pulse from which the presence of consciousness can be inferred with unprecedented sensitivity (low false alarm rate), and specificity (low miss rate), at the level of individual patients.

PCI has been comprehensively studied and validated in humans since its introduction by Massimini and colleagues in 2005 (Casali et al., 2013; Casarotto et al., 2016; Comolatti et al., 2019; Ferrarelli et al., 2010; Massimini et al., 2005; Rosanova et al., 2018). Pigorini et al. (2015) proposed that during non-rapid eye movement (**NREM**) sleep, when the brain is characterized by cortical bistability, neurons tend to fall into a down-state following activation (either endogenous or exogenous) preventing extended causal interactions that are typical during wakefulness (Hill & Tononi, 2005; Rosanova et al., 2018; Timofeev et al., 2001).

Limitations in access to high resolution cellular recordings in humans have motivated recent efforts to translate the PCI technique to model systems for more detailed studies of the circuit mechanisms underlying complexity changes. In 2018, D'Andola et al. demonstrated that an approximation of PCI developed for *in vitro* measurements captured complexity differences in ferret cortical slices exhibiting sleep- and awake-like activity patterns. They showed that during a sleep-like state, electrical stimulation induced a down-state that disrupted the complex pattern of activation observed in the awake-like state (D'Andola et al., 2018). Arena et al. (2021) were the first to recapitulate the human PCI results *in vivo* in rodents; they computed the complexity of electrically evoked EEG responses in rats and showed that PCI was high during wakefulness and low during anesthesia. In their comprehensive study, they found that in the anesthetized state (via propofol or sevoflurane), stimulation was followed by a widespread suppression of high frequencies in the EEG responses, suggestive of a down-state, in agreement with previous findings (D'Andola et al., 2018; Pigorini et al., 2015). Dasilva et al. (2021) measured PCI *in vivo* in anesthetized mice and showed that complexity can be modulated even within the anesthetized state. They showed that PCI was highest for mice under light isoflurane anesthesia (defined as a concentration of 0.1%), decreasing systematically at medium (0.34%) and deep (1.16%) concentrations. While pioneering, none of these studies simultaneously recorded many neurons and brain regions to analyze the circuits underlying the macroscopic electrical responses.

To investigate how cortico-cortical and cortico-thalamic activity influences the complexity of the evoked responses, we used EEG simultaneously with Neuropixels probes to record brain-wide evoked responses to cortical electrical stimulation in head-fixed mice that were awake and, subsequently, anesthetized with isoflurane. Due to their ability to record hundreds of neurons across all cortical layers and subcortical structures, Neuropixels probes provide unprecedented access to the intra- and interareal dynamics that underlie the macro-scale EEG signals. We show that cortical stimulation elicits a widespread, complex event-related potential (**ERP**) in the EEG signals in the awake state, but a much simpler ERP in the anesthetized state, in agreement with what has been shown in humans (Casali et al., 2013) and rats (Arena et al., 2021). We demonstrate a stereotyped pattern of activity to stimulation in deep (but not superficial) cortical layers – brief excitation, followed by a profound *off* period and a *rebound* excitation. This sequence is repeated in the thalamus, supported by burst firing in excitatory thalamic neurons. Based on relative timing between cortical and thalamic evoked activity, we infer that thalamic bursting is necessary for the late, evoked EEG component seen in response to electrical stimulation, a novel result that links the ERP to activity in the cortico-thalamo-cortical (**CTC**) loop.

RESULTS

Global evoked responses are modulated by the depth of the cortical stimulation site

We recorded global EEG-like neural signals using a multi-electrode surface array on the skull, but below the scalp (Jonak et al., 2018; Land et al., 2019), in head-fixed mice. The multi-electrode array consisted of 30 electrodes situated over primary and secondary motor, somatosensory, visual, and retrosplenial areas in both hemispheres (Figure 1A). We used an average reference montage that removed signals common to all EEG electrodes (see Methods). We inserted a bipolar wire electrode intra-cortically to repeatedly deliver a single electrical current pulse into the cortex and measured the evoked potentials with the EEG array (Figure 1B-C). The current pulses were biphasic (200 µs/phase), charge-balanced, and cathodic-first, with a current amplitude between 10-100 µA (Figure 1C inset). Stimulation artifacts in the EEG signals were reduced by replacing the signal between 0 and +2 ms following each stimulus with the signal between -2 and 0 ms; this was done to all traces in all trials during an offline, signal pre-processing step. All subsequent analysis of the ERP excludes the signal between -2 and +2 ms. During the experiment, we closely observed the animal for signs of electrically evoked motor twitches and chose lower stimulation amplitudes if we observed any.

To understand how the features of the ERP depend on the location of the electrical stimulation, we varied both the area and the depth (or cortical layer) of the stimulating electrode. We stimulated in the secondary motor area (**MOs**) and the primary somatosensory area (**SSp**) in layer 2/3 (superficial: 0.41±0.04 mm below the brain surface) and layer 5/6 (deep: 1.06±0.05 mm below the brain surface) (Figure 1D). We found that regardless of area, when we stimulated layer 5/6 during the awake period, we usually observed two prominent peaks in the ERP: an initial response around 25 ms and secondary peak at around 180 ms post-stimulation (Figure 1C and 1D).

The early component was preserved, whereas the second, late component was not evident when stimulating superficially in either area (Figure 1D). The total duration of the ERP was not significantly different when stimulating superficial layers compared to deep layers (mean ERP duration for superficial stimulation: 0.4±0.0 s; deep stimulation: 0.5±0.1 s; Student's two-tailed t-test, p=0.05; Figure 1E). When stimulating superficially, ERPs had a significantly smaller normalized magnitude compared to stimulating deep layers (mean ERP magnitude for superficial stimulation: 3.3±0.8; deep stimulation: 6.6±0.9; Student's two-tailed t-test, p=0.02; Figure 1F).

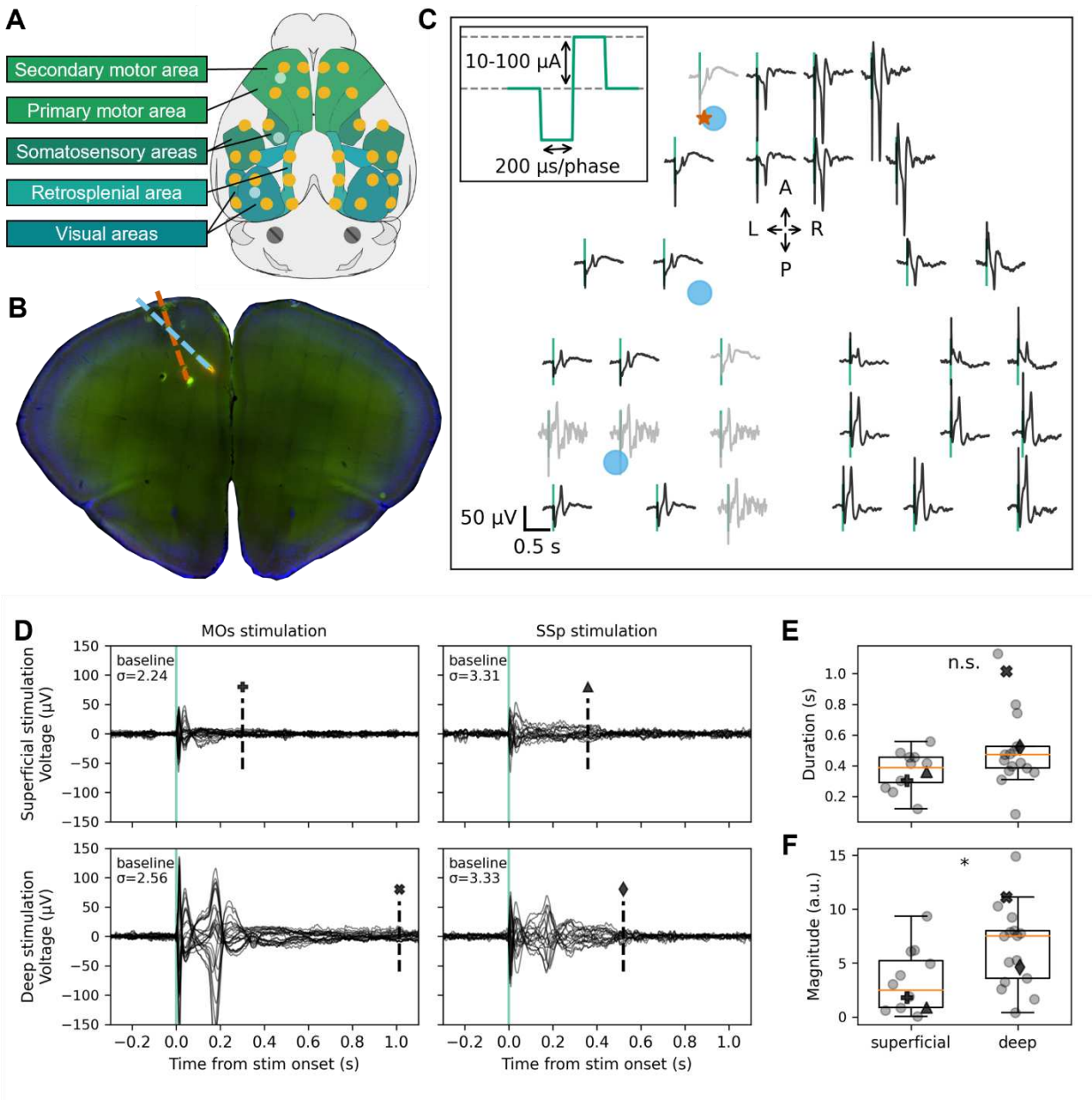

Figure 1: Evoked EEG responses in awake, head-fixed mice.

(A) Schematic of the 30-channel surface array (yellow dots) implanted on top of the skull over major brain areas: motor, somatosensory, retrosplenial, and visual areas (schematic created using brainrender, Claudi et al., 2021). The circular, platinum EEG electrodes are 500 µm in diameter. The three light blue circles correspond to the locations of the three acute craniotomies to place the bipolar stimulating electrode and, up to three, Neuropixels probes. The schematic also shows two skull screws over the cerebellum that serve as the reference and the ground for the EEG signals. **(B)** Histological image of a coronal brain slice showing the location of the bipolar stimulating electrode (spanning MOs, layer 5; red dashed line) and one of the Neuropixels probes (spanning layers of MOs and anterior cingulate areas; blue dashed line) with fluorescent dyes (that appear red and green in the image). **(C)** Evoked responses from each of the 30 EEG electrodes from the awake, head-fixed mouse from -0.2 to +0.8 s following the electrical stimulus (vertical green line marks the onset time). Traces are arranged in the approximate orientation of the EEG array over the skull surface. Traces in black and gray represent signals that did and did not

pass a quality control step, respectively. The red star and blue circles mark the approximate insertion point of the bipolar stimulating electrode and the Neuropixels probes, respectively. **(D)** Evoked responses (-0.2 to +0.8 s around stimulus onset) with all EEG electrode traces superimposed (butterfly plots). Each of the four panels represents data from a different stimulated area and depth: top and bottom left – superficial and deep layer (same as in panel C) of MOs in the same subject; top and bottom right – superficial and deep layer of SSp in a different subject. The dashed vertical line indicates the duration of the evoked signal; the marker above matches with the marker representing the value in panels **E** and **F**. The "baseline σ" indicates the standard deviation (in μV) over all electrodes during the 2 s preceding the stimulus. **(E)** Duration of the EEG ERPs for all subjects based on the stimulation depth: superficial (N=12 mice) vs. deep (N=17 mice). **(F)** Normalized magnitude of the EEG ERPs for all subjects based on the stimulation depth: superficial (N=12 mice) vs. deep (N=17 mice). For further details, see method "ERP duration and magnitude" and Figure S2. Boxplots show median (orange line), 25th, and 75th percentiles; whiskers extend from the box by 1.5x the inter-quartile range (IQR). * $p < 0.05$, ** $p < 0.01$, *** $p < 0.001$.

The magnitude of the first peak in the EEG decays systematically when moving away from the stimulation site until it eventually flips its sign, most likely reflecting volume conduction (Figure S1). The magnitude and polarity of the second component likewise changes continuously but in a different pattern (Figure S1), suggesting a different mechanistic origin.

The spiking response pattern of the stimulated cortex echoes the ERP

In addition to recording EEG signals, we simultaneously collected data from up to three Neuropixels probes – linear silicon probes with a 10 mm long non-tapered shank with 384 simultaneously recorded electrodes capable of capturing local field potential (**LFP**) and action potentials (Jun et al., 2017). The Neuropixels probes were placed in such a manner as to record from cortex (motor **MO**, anterior cingulate **ACA**, somatosensory **SS**, and visual **VIS**) and sensorimotor-related thalamic nuclei (**SM-TH**, Figure 2A), see full list of thalamic nuclei in the Methods section (Guo et al., 2017; J. A. Harris et al., 2019; Hooks et al., 2013). This allowed us to observe the LFP and spiking activity of hundreds of individual cortical and thalamic neurons. Because we inserted a Neuropixels probe near the stimulating electrode (within 0.5 mm) and, often, up to two more Neuropixels probes at distal locations, we observed direct responses (i.e., here defined operationally as neurons that spike between 2-25 ms following the electrical pulse; this might miss a handful of very rapidly responding neurons; see Sombeck et al., 2022; Stoelzel et al., 2009) and indirect responses to the electrical stimulation.

When we stimulated superficial MOs, we observed a locally evoked LFP response as well as a brief period of spiking followed by a period of inhibition lasting 94.2±16.1 ms in MO neurons (Figure 2B-2D, left). We observed minimal to no evoked responses (LFP or spikes) in other sampled areas. When we stimulated deep MOs, we observed a robust evoked LFP response accompanied by spiking activity that was reflective of the two components in the ERP: an initial excitation within 25 ms (peak population firing rate 38.1±4.2 Hz), followed by a period of inhibition (duration 125.0±5.5 ms), followed by a longer period of strong excitation (peak population firing rate 7.9±0.7 Hz; Figure 2B-2D, right). This cortical spiking response pattern following deep stimulation is quite stereotyped – an initial excitation, followed by an off period and a strong rebound excitation. We seldom observed this pattern for superficial stimulation (Figure 2C and 2D, left). Indeed, on average, about three times more cortical neurons respond significantly for deep than for superficial stimulation (Figure 4A).

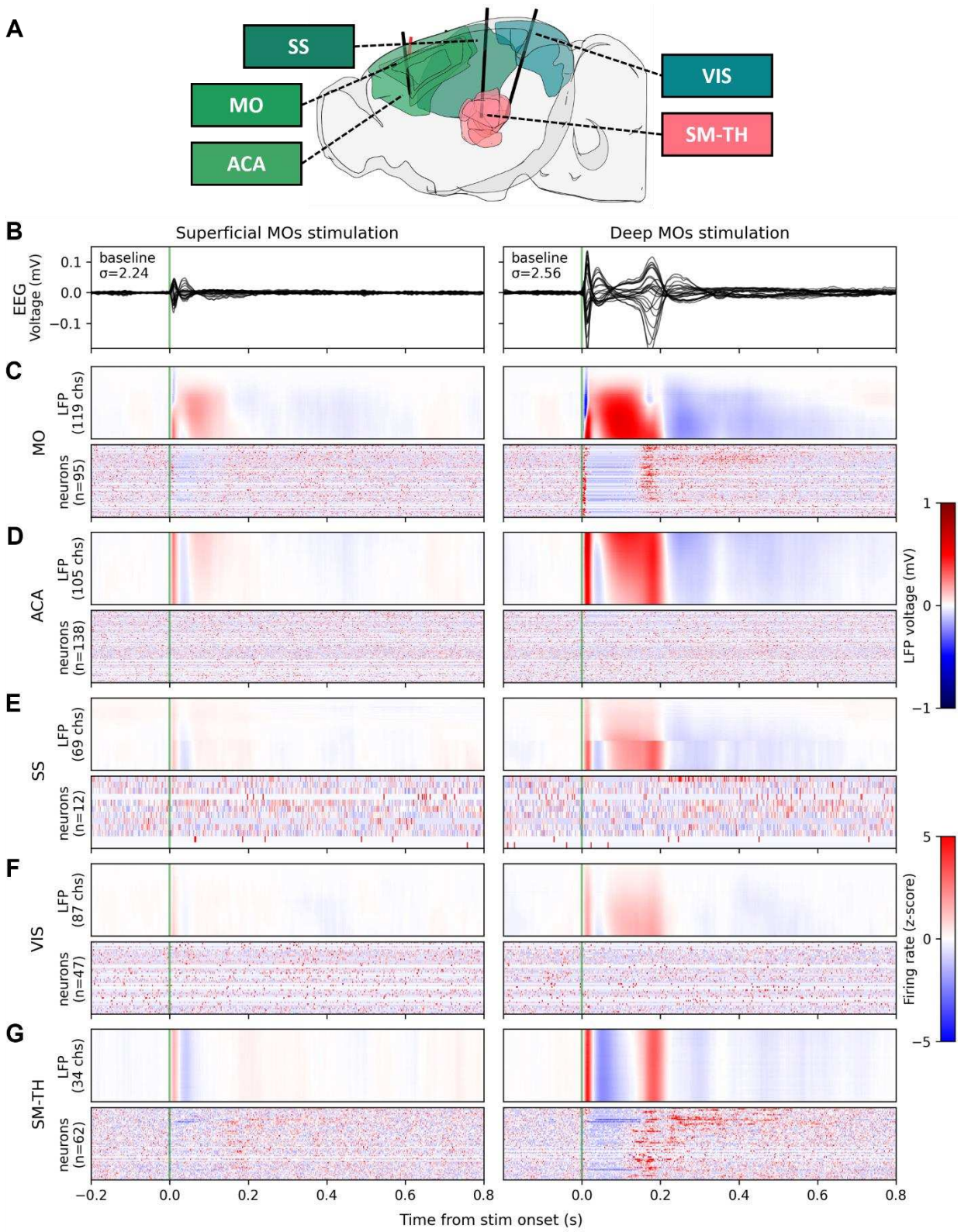

Figure 2: Single pulse electrical stimulation evokes strong responses in the EEG, LFP, and in some populations of neurons (locally in motor cortex and in SM-TH) when deep layers of MOs are directly activated.

(A) Sagittal view of a schematic of the mouse brain highlighting areas of interest: motor (MO), anterior cingulate (ACA), somatosensory (SS), visual (VIS), and somatomotor-related thalamic (SM-TH) areas (schematic created using brainrender, Claudi et al., 2021). The solid black lines show the approximate locations of three Neuropixels probes acutely inserted to record single neuron activity and local field potentials. The approximate location of stimulating electrode in the deep layers of MOs is shown in red. **(B)** Butterfly plots of evoked EEG responses (-0.2 to +0.8 s around stimulus onset) during the awake state. Each column represents data from a different stimulated depth (superficial and deep MOs) in the same subject (same subject shown in Figure 1D left top and bottom). **(C)** Evoked responses from the Neuropixels electrodes in MO. **Top:** Evoked responses measured by the Neuropixels LFP band in mV. The signals from all electrodes within the targeted region are represented as a heat map (red colors are positive voltages and blue colors are negative). The number of Neuropixels electrodes (chs) in each area is included along the y-axis. **Bottom:** Normalized firing rate, reported as a z-score of the average, pre-stimulus firing rate, of all RS neurons recorded by the Neuropixels probes targeting the area of interest. The number of neurons (n=) in each area is included along the y-axis. **(D)** Evoked responses from the ACA, same information as panel **C**. **(E)** Evoked responses from the SS, same information as panel **C**. **(F)** Evoked responses from the VIS, same information as panel **C**. **(G)** Evoked responses from the SM-TH, same information as panel **C**.

Global ERPs are not associated with widespread evoked cortico-cortical spiking activity

Intrigued by the apparent lack of firing rate changes in non-stimulated cortical regions, we quantified the significance and the absolute magnitude of both LFP and spiking responses for each cortical area in response to superficial and deep stimulation (note that our magnitude metric accounts for both reductions as well as increases in firing; see method “LFP and population spiking magnitude”; Figure 3A and 3B). The magnitude of the LFP near the stimulation site increases compared to baseline (10.1 times baseline magnitude) and decays with distance from the stimulation site (4.8 times baseline in visual cortex; Figure 3A). Yet while we see large and highly significant deviation in firing of cortical neurons (3.1 times baseline magnitude) close to the stimulation electrode, changes in firing become marginal and not significant away from the cortical stimulation site (Figure 3B).

We observed significant evoked LFP responses in the stimulated cortical region in all subjects regardless of the stimulation depth (superficial: 6/6 mice; deep: 15/15 mice; Figure 3C), as well as for all non-stimulated regions (superficial: 7/7 mice; deep: 16/16 mice). Regarding cortical spiking, we mainly observed significant responses locally resulting from deep stimulation (14/15 mice), but not always from superficial stimulation (1/6 mice). Non-stimulated cortical regions rarely had significant evoked spiking responses regardless of stimulation depth (superficial stimulation: 1/7 mice; deep stimulation: 2/16 mice). The largest evoked LFP and population spiking responses were recorded in stimulated cortex following from deep stimulation (LFP magnitude: stimulated median 9.2 [7.8-10.8 IQR], non-stimulated median 5.1 [4.0-7.0 IQR]; population spiking magnitude: stimulated median 3.1 [2.3-3.4 IQR], non-stimulated median 1.3 [1.2-1.7 IQR]; Figure 3D). We found a highly significant positive relationship between the amplitude of the evoked LFP and the amplitude of the evoked population firing rate in non-stimulated cortical regions. Together, these data show that cortical stimulation evoked widespread changes in the LFP, but rarely evoked ipsilateral cortical spiking activity outside of the stimulated area.

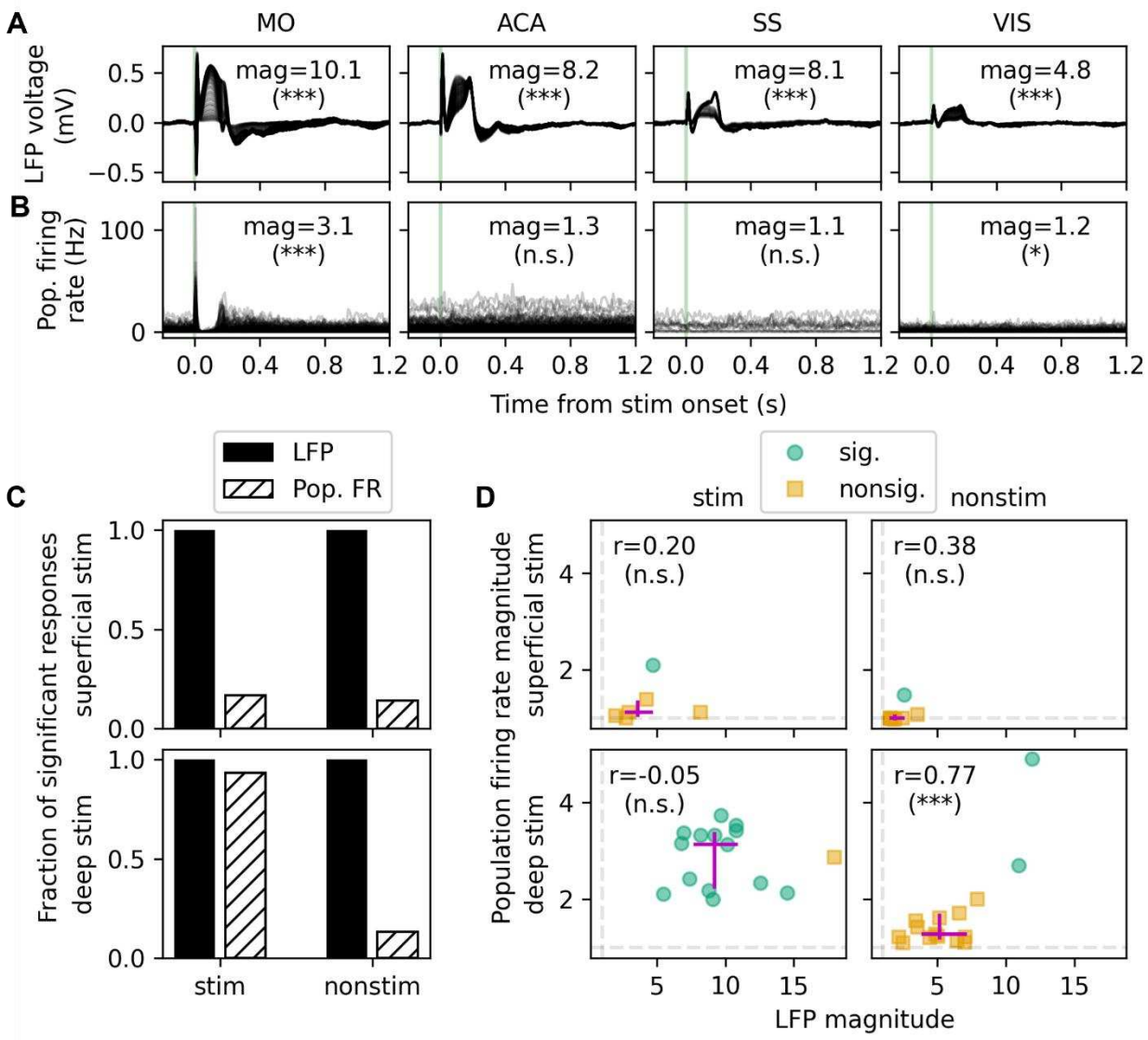

Figure 3: Widespread evoked responses are seen in the LFP signals but not always in evoked firing rate changes when stimulating deep layers of the ipsilateral cortex.

(A) Evoked LFP responses (-0.2 to +1.2 s around stimulus onset) from deep MOs stimulation (same subject as Figure 1D bottom left), all recorded cortical sites along the Neuropixels shaft are superimposed. Each column represents data from a different targeted cortical area (MO, ACA, SS, and VIS). The magnitude (mag=) is computed as the integrated area of the response divided by the integrated area of the baseline. **(B)** Evoked neuronal firing rates from deep MOs stimulation (same subject as above), each trace represents a single regular spiking neuron. Each column represents data from a different targeted cortical area (MO, ACA, SS, and VIS). **(C)** Fraction of significant evoked LFP (black shaded) and population spiking (diagonal hatch) responses from stimulated (stim) and non-stimulated (nonstim) cortical regions resulting from superficial stimulation (top) and deep stimulation (bottom). Superficial stimulation: n=6 stimulated cortical regions in N=6 mice and n=17 non-stimulated cortical regions in N=7 mice. Deep stimulation: n=15 stimulated cortical regions in N=15 mice and n=35 non-stimulated cortical regions in N=16 mice. **(D)** Magnitude of evoked LFP and population spiking response for superficial (**top**) and deep stimulation (**bottom**) for stimulated (stim, **left**) and non-stimulated cortical areas (nonstim, **right**). Green circles and orange squares represent regions with significant and non-significant evoked spiking responses,

respectively, because all evoked LFP responses were significant. The light gray vertical and horizontal dashed lines represent response to baseline magnitude equal to one. The magenta crosshairs represent the median values (point of intersection) and the interquartile ranges (25^{th} and 75^{th} percentiles). A line was fit to each dataset and the slope (r) and p-value (p) are represented in each panel, * $p < 0.05$, ** $p < 0.01$, *** $p < 0.001$.

To further investigate the evoked neural spiking responses across both stimulated and non-stimulated cortical areas, we computed the percentage of modulated (significantly increased or decreased spiking relative to the pre-stimulus baseline) regular spiking (**RS**) neurons (putative pyramidal neurons) in three temporal windows following the stimulus: 2-25 ms (initial excitation), 25-150 ms (off period), and 150-300 ms (rebound excitation; Figure 4). The three temporal windows were chosen to match the stereotyped firing patterns observed in several subjects, which align with maximum peaks in the ERPs and the period in between (Figure S1). We separately analyzed fast spiking (**FS**) neurons and found they behave like RS neurons (Figure S3), therefore further analyses focus only on RS neurons.

During the initial excitation, the fraction of activated (significantly increased spiking relative to baseline) neurons was always higher in the stimulated cortex than other cortical areas, for both superficial and deep stimulation. The fraction of activated neurons in non-stimulated cortical regions was only minimally above zero (Figure 4A and 4D). Indeed, across all N=23 animals, only 0.4% (minimum 0%, maximum 2.3%) of the neurons were modulated in the initial excitation, compared to 16.7% (minimum 0%, maximum 100%) in stimulated cortex.

Next, we quantified the fraction of modulated RS neurons in the off period between 25 and 150 ms, capturing the period between the two large ERP amplitude components that were usually present (with deep stimulation). There were very few neurons with increased spiking in this temporal window, regardless of stimulation depth and stimulated or non-stimulated area (mean 0.4%, minimum 0%, maximum 2.8%; Figure 4B and 4E). In contrast, spiking activity in 16/21 animals was significantly reduced from baseline values following either superficial or deep stimulation. Interestingly, some non-stimulated areas showed decreased spiking activity but only in response to deep stimulation (mean 12.1%, minimum 0%, maximum 45.4%).

The final temporal window we considered was between 150 and 300 ms, coinciding with the second component in the ERP. All 15 subjects who received deep stimulation showed significant rebound excitation in the stimulated cortex, whereas only 1/6 superficial stimulation subjects did (Figure 4C and 4F). Some subjects who received deep stimulation showed significant rebound excitation in the non-stimulated areas (8/15 animals; Figure 4F), but it was less common amongst the superficial stimulation subjects (1/7 animals; Figure 4C).

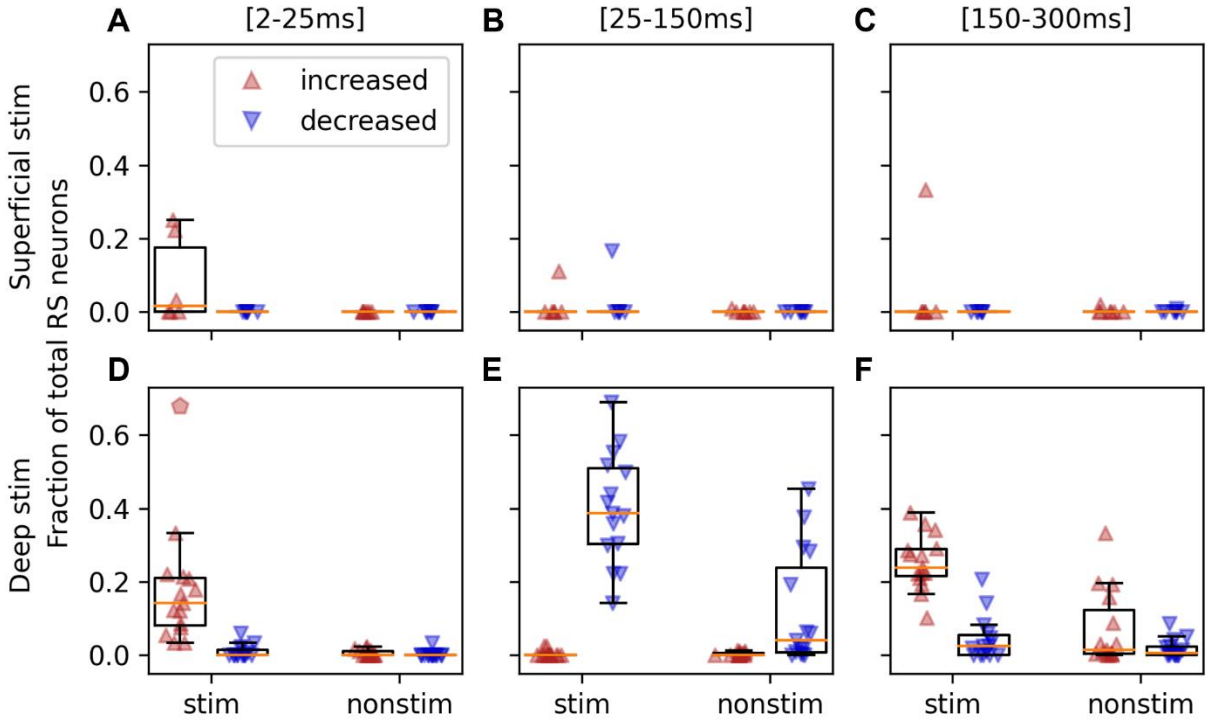

Figure 4: The fraction of the neuron population that is significantly modulated depends on the layer of stimulation.

(A) The fraction of RS neurons that exhibit a significantly increased (red upward triangle) or decreased (blue downward triangle) response in the first 25 ms for mice that received superficial stimulation. **(B)** The fraction of RS neurons that exhibit a significantly increased or decreased response 25-150 ms following the stimulus. **(C)** The fraction of RS neurons that exhibit a significantly increased or decreased response 150-300 ms following the stimulus. **(D-F)** Same as panels **A-C** but for deep stimulation. The red pentagon in panel **D** represents one outlier in which all RS neurons have a significantly increased response. Panels **A-C** represent experiments using superficial cortical stimulation (**top**, 870 RS neurons from stimulated cortex and 4,110 RS neurons from non-stimulated cortical regions in N=7 mice) and panels **D-F** represent experiments with deep cortical stimulation (**bottom**, 2,442 RS neurons from stimulated cortex and 8,313 RS neurons from non-stimulated cortical regions in N=15 mice). Boxplots show median (orange line), 25th, and 75th percentiles; whiskers extend from the box by 1.5x the IQR.

Cortico-thalamo-cortical interactions underlie features of the ERPs

The striking tri-phasic cortical spiking pattern for deep stimulation is replicated in the associated thalamic nuclei that are connected to the stimulated cortical area (here SM-TH; Guo et al., 2017; Harris et al., 2019; Hooks et al., 2013; bottom right in Figure 2D), though with different timing. Specifically, we observed a brief excitation (peak population firing rate 22.3±3.2 Hz), a 74.6±15.5 ms long period of suppression, followed by rebound excitation (peak population firing rate 14.7±1.0 Hz). This is not the case when stimulating superficial layers (bottom left in Figure 2C and 2D).

We quantified the fraction of significantly modulated neurons in the SM-TH population and found that the neurons were 30 times more likely to be modulated by deep than superficial stimulation (superficial:

1.1±1.5% of SM-TH population, N=3 mice; deep: 33.5±17.1%, N=12 mice; Student's two-tailed t-test, p=0.009; Figure 5A).

Further exploration of the thalamic response revealed bursts of action potentials during the rebound (Figure 5B); bursting is a well-known activity mode of thalamic relay cells and is defined as two or more consecutive spikes with an inter-spike interval less than 4 ms preceded by a period of quiescence of at least 100 ms (Contreras & Steriade, 1995; Grenier et al., 1998; Guido & Weyand, 1995; Halassa et al., 2011; Lu et al., 1992; Nestvogel & McCormick, 2021). We quantified the average burst probability (75-300 ms after stimulus onset) and found that deep stimulation had a significantly higher likelihood of evoking bursts (superficial stimulation: median 0 [0-0.03 IQR]; deep stimulation: median 0.14 [0.02-0.21 IQR]; Mann-Whitney *U* test, p=0.026; Figure 5C).

We hypothesized that deep stimulation elicits cortical spiking of cortico-thalamic projection neurons followed, with some delay due to axonal propagation and synaptic transmission, by thalamic neurons, whereas during the rebound period thalamic bursting will precede cortical rebound spiking. Accordingly, we evaluated the median time-to-first-spike for the population in the 2-25 and 75-300 ms intervals (Figure 5D). During the initial excitation, stimulated cortical RS cells had a median first-spike latency of 4.5±0.9 ms, with the thalamic population following at 11.1±2.8 ms (mean latency difference of 6.7 ms; paired t-test, p=1.7E-5; Figure 5E). During the rebound excitation window, the temporal relationship flipped: the thalamic population had a median rebound spike latency of 148.4±22.1 ms, with cortex following at 185.4±17.5 ms (mean latency difference -37.0 ms; paired t-test, p=4.2E-4; Figure 5F).

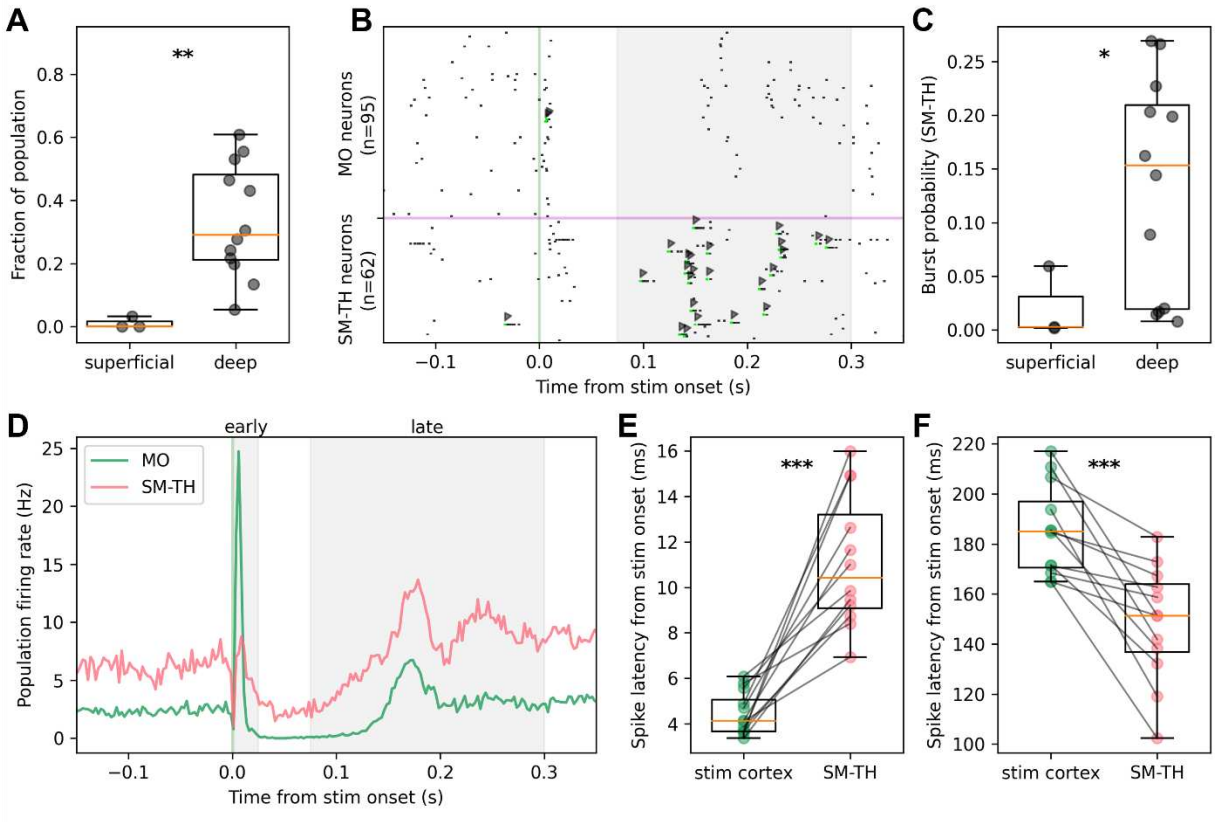

Figure 5: The second component in the ERP is associated with thalamic burst firing and thalamo-cortical interactions.

(A) The fraction of neurons that exhibit a significantly increase or decrease to the stimulation in the 300 ms following the stimulus for the SM-TH for superficial (N=3 mice) and deep stimulation (N=12 mice). **(B)** A single trial raster showing spiking activity of MO (top) and SM-TH neurons (bottom) in response to a single deep pulse (at the green vertical line). Many of the SM-TH discharges appear as bursts of action potential (green marks flagged with arrows), especially during the rebound response window. **(C)** The probability (fraction of total trials) that the SM-TH produces bursts within 75-300 ms from stimulus onset. There was a higher likelihood of observing SM-TH bursts resulting from deep cortical stimulation (superficial, N=3 mice; deep, N=12 mice). **(D)** The population firing rate (trial-averaged) for MO (green) and SM-TH (pink) (-0.15 to +0.35 s) for one example subject with deep MOs stimulation (same subject as in Figure 1D bottom left). **(E)** The latency to first-spike (2-25 ms) for responsive RS neurons in stimulated cortex (green circles) and in the associated SM-TH (pink circles). Populations are recorded simultaneously in each subject, represented by the connecting black lines (N=12 mice). **(F)** The latency to spike in the late window (75-300 ms) for responsive RS neurons in stimulated cortex (green circles) and in the SM-TH (pink circles). Populations are recorded simultaneously in each subject, represented by the connecting black lines (N=12 mice). Boxplots show median (orange line), 25^{th}, and 75^{th} percentiles; whiskers extend from the box by 1.5x the IQR. * $p < 0.05$, ** $p < 0.01$, *** $p < 0.001$.

Because thalamic bursts powerfully activate cortical neurons (Nestvogel & McCormick, 2021; Ramcharan et al., 2005; Sherman, 1996) and EEG signals are a read-out of cortical activity, we sought to investigate the relationship between thalamic bursting, cortical spiking, and the ERP. We computed the correlation between these metrics in the rebound window (75-300 ms after stimulus onset) on a trial-by-trial basis for each subject. The fraction of bursting SM-TH neurons was highly correlated with the cortical population firing rate (8/12 mice with a significant correlation [$p<0.05$], mean Pearson r value: 0.4±0.04; Figure 6A and 6B). The cortical population firing rate was highly correlated with the magnitude of the second, late component in the ERP (9/12 mice with a significant correlation [$p<0.05$], mean Pearson r value: 0.5±0.04; Figure 6C and 6D). Additionally, the late component in the ERP was significantly correlated with the fraction of bursting SM-TH neurons (12/12 mice with a significant correlation [$p<0.05$], mean Pearson r value: 0.4±0.08; Figure S4A and S4B), much more so than it was correlated with the SM-TH population firing rate (Figure S4C and S4D). These are important observations linking a micro-variable (cellular thalamic bursting) with a macro-variable (cortical EEG).

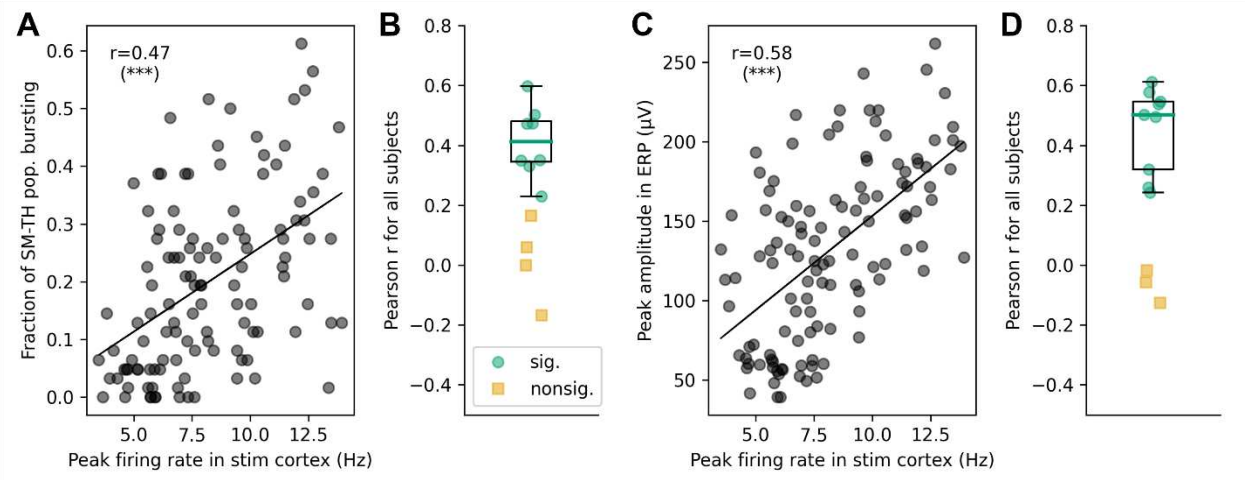

Figure 6: The amplitude of the second, late component in the ERP is correlated with the cortical population firing rate, which is correlated with thalamic burst firing.

(A) The Pearson correlation between the fraction of the SM-TH that bursts and the peak cortical population firing rate on a trial-by-trial basis for one example mouse (same subject as in Figure 1D bottom left). **(B)** The correlation value (Pearson r) for the comparison in panel **A** for all subjects with deep stimulation (N=12 mice), green circles represent subjects with a significant correlation ($p<0.05$) and yellow squares represent subjects with a non-significant correlation. **(C)** The Pearson correlation between the peak amplitude of the second, late component in the ERP and the peak cortical population firing rate on a trial-by-trial basis for one example mouse (as in panel **A**). **(D)** The correlation value (Pearson r) for the comparison in panel **C** for all subjects with deep stimulation (N=12 mice), represented as in panel **B**. Boxplots show median (green line), 25th, and 75th percentiles; whiskers extend from the box by 1.5x the IQR. * $p < 0.05$, ** $p < 0.01$, *** $p < 0.001$.

Behavioral states modulate the ERP and the cortico-thalamic interactions

To study differences between the evoked responses across conscious and unconscious states, we performed experiments on mice that were awake and subsequently anesthetized via isoflurane. At the start of an experiment, we delivered up to 120 single electrical pulses while the mouse was awake, free to rest or run on a freely moving wheel. Next, we induced anesthesia with isoflurane via inhalation. Once the mouse reached a stable level of unconsciousness (no reaction to an alcohol swab placed in front of the nose; 4.0±0.4 min after induction onset at 5% isoflurane concentration), we delivered the same set of electrical stimuli.

We separated each trial by behavioral state based on whether the animal was stationary (*quiet wakefulness*) or running (*active wakefulness*, defined here as an average running speed exceeding 0 cm/s in a window from -0.5 to 0.5 s from the stimulation onset). We then compared average responses from 98 (median, [85-104 IQR]) quiet wakefulness, 21 (median, [15-28 IQR]) active wakefulness, and 120 (median, [119-120 IQR]) anesthetized trials across 16 animals. Both locomotion and anesthesia clearly modulated the ERPs (Figure 7A) and the evoked firing rates of cortical and thalamic neurons (Figure 7B). The second component in the ERP is clearly diminished when running and nonexistent during anesthesia; this is captured by the decrease in ERP duration (quiet wakefulness 0.6±0.1 s, running 0.3±0.0 s, anesthetized 0.3±0.0 s; one-way repeated measures (RM) ANOVA, state effect: $F(2, 30)=10.5$,

p=3.0E-4; Figure 7C) and magnitude (quiet wakefulness 6.4±0.9, running 1.7±0.3, anesthetized 1.7±0.3; Friedman test, state effect: Q(2)=15.9, p=3.6E-4; Figure 7D).

Next, we examined how cortical and thalamic activity differed as a function of behavioral state. In both regions, the baseline firing rates (measured during the pre-stimulus epoch) were higher during running and lower during anesthesia compared to quiet wakefulness (stimulated cortex baseline firing rate: N=15 mice, quiet wakefulness 3.3±0.2 Hz, running 5.0±0.5 Hz, anesthetized 1.1±0.2 Hz; one-way RM ANOVA, state effect: F(2, 28)=61.4, p=1.6E-8, Figure 7E left; SM-TH baseline firing rate: N=12 mice, quiet wakefulness 9.4±1.5 Hz, running 16.8±1.6 Hz, anesthetized 0.8±0.4 Hz; Friedman test, state effect: Q(2)=22.2, p=1.5E-5, Figure 7E right).

The median first spike latencies for cortical and thalamic populations were the same when looking at the initial excitation (N=12 mice; stimulated cortex latency: quiet wakefulness 4.5±0.3 ms, running 4.1±0.3 ms, anesthetized 4.5±0.5 ms; SM-TH latency: quiet wakefulness 11.3±0.8 ms, running 11.1±0.8 ms, anesthetized 10.7±0.6 ms; two-way RM ANOVA, state effect: F(2, 22)=0.4, p=0.6, region effect: F(1, 11)=78.7, p=2.0E-6, interaction: F(2, 22)=0.3, p=0.6; Figure 7F). However, the rebound spike latencies for cortex and thalamus were earlier during running compared to quiet wakefulness (N=12 mice; stimulated cortex latency: quiet wakefulness 187.9±4.8 ms, running 166.4±4.7 ms, anesthetized 203.2±7.5 ms; SM-TH latency: quiet wakefulness 156.6±7.7 ms, running 123.0±4.3 ms, anesthetized 197.5±10.0 ms; two-way RM ANOVA, state effect: F(2, 22)=29.3, p=5.7E-5, region effect: F(1, 11)=16.8, p=0.002, interaction: F(2, 22)=6.3, p=0.017; Figure 7G). The cortex and thalamus did not exhibit consistently timed rebound excitation during anesthesia, so the relative timing during this state was random and often later than during quiet and active wakefulness. The probability of evoking thalamic bursts decreased during running compared to quiet wakefulness and was very low (zero for many subjects) during anesthesia (N=12 mice; median probability: quiet wakefulness 0.1 [0.01-0.24 IQR], running 0 [0-0.07 IQR], anesthetized 0 [0-0.002 IQR]; Friedman test, state effect: Q(2)=16.7, p=2.4E-4; Figure 7H).

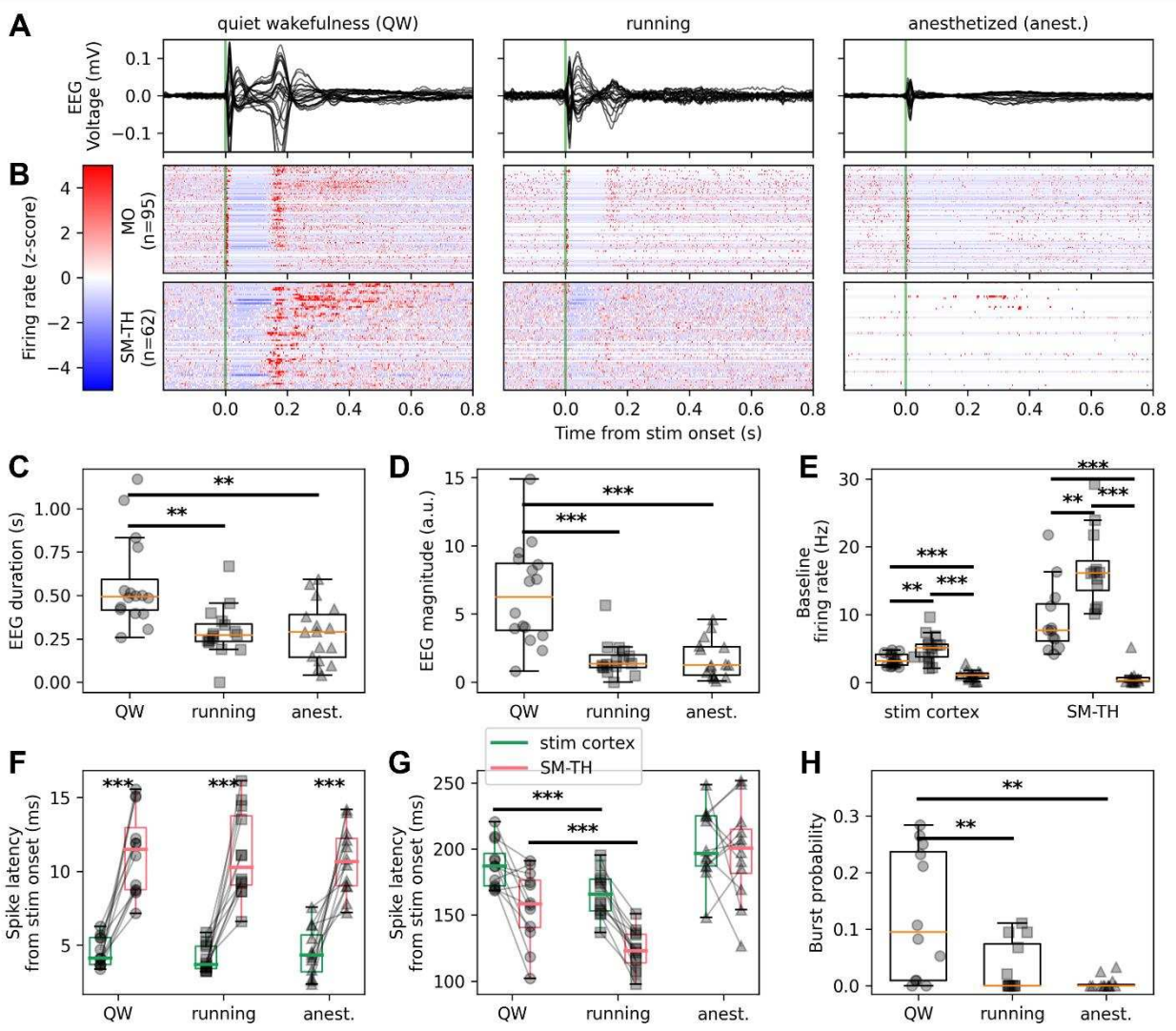

Figure 7: Brain state modulates the ERP via CTC interactions.

(A) Butterfly plot of ERPs during the non-running (quiet wakefulness), running (active wakefulness) and the isoflurane-anesthetized states (same subject as in Figure 1D bottom left). **(B)** Normalized firing rate, reported as a z-score of the average, pre-stimulus firing rate, of all RS neurons recorded by the Neuropixels probes targeting the stimulated cortex (MO) and SM-TH (same subject as in Figure 1D bottom left). **(C)** Duration of the ERPs for all states (see also Figure 1E top): quiet wakefulness, running, and anesthetized (N=16 mice). **(D)** Magnitude of the ERPs for all states (see also Figure 1E bottom): quiet wakefulness, running, and anesthetized (N=16 mice). **(E)** Baseline firing rates of cortical (stim cortex) and SM-TH neurons across all states (stim cortex: N=15 mice; SM-TH: N=12 mice). **(F)** The latency to first-spike (2-25 ms) for responsive RS neurons in the stimulated cortex (green circles) and in the SM-TH (pink circles) across all states. Populations are recorded simultaneously in each subject, represented by the connecting black lines (N=12 mice). **(G)** The latency to spike in the late window (100-300 ms) for responsive RS neurons in the stimulated cortex (green circles) and in the SM-TH (pink circles) across all states. Populations are recorded simultaneously in each subject, represented by the connecting black lines. **(H)** The probability (fraction of total trials) that the SM-TH produces AP bursts within 75-300 ms from the stimulus onset for the three states (N=12 mice). Boxplots show median, 25th, and 75th percentiles; whiskers extend from the box by 1.5x the IQR. * $p < 0.05$, ** $p < 0.01$, *** $p < 0.001$.

Thus, thalamic activity preceded cortical activity during the rebound excitation in both quiet and active wakefulness. However, during quiet wakefulness the rebound is characterized by thalamic burst firing, which correlated with increased cortical spiking and higher ERP magnitudes (Figure 6).

Thalamo-cortical interactions affect perturbational complexity in head-fixed mice

The differences of ERPs we observed across behavioral states, which reflected differences in the cortico-cortical and cortico-thalamic interactions as described above, resulted in significant changes in complexity across states (Figure 8A). To quantify complexity, we used an algorithm that quantifies the number of state transitions for each principal component in the ERP (**PCI^{ST}**; Comolatti et al., 2019). Like the PCI, this metric distinguishes conscious from unconscious states in a variety of human volunteers and patients with disorders of consciousness (Comolatti et al., 2019) as well as rats (Arena et al., 2021); unlike PCI, PCI^{ST} does not require source modeling and is not upper-bounded by 1. When PCI^{ST} is high, signals are both spatially and temporally differentiated. When it is low, signals are highly correlated across space and time or very small relative to the pre-stimulus signal. We found that PCI^{ST} was higher during the awake state than during the anesthetized state in all subjects (N=30 mice; awake PCI^{ST} 46.0±3.7; anesthetized PCI^{ST} 16.8±2.5; paired t-test, p=6.8E-11; Figure 8B).

Based on our observation that superficial stimulation evoked simpler responses than deep stimulation (in the awake state), we found that PCI^{ST} was, indeed, significantly lower for superficial than for deep stimulation (superficial: N=13 mice, awake PCI^{ST} 35.6±4.8; deep: N=17 mice, awake PCI^{ST} 53.9±4.5; Student's two-tailed t-test, p=0.013; Figure 8C).

To compare PCI^{ST} during quiet and active wakefulness, and anesthesia, we selected subjects that had at least 30 running trials since averaging the ERP over too few trials can affect the PCI^{ST} calculation (Comolatti et al., 2019). PCI^{ST} was significantly different for all states; the highest complexity ERPs were seen when mice were in quiet wakefulness, slightly lower complexity ERPs during active wakefulness, with the lowest complexity during anesthesia (N=8 mice; quiet PCI^{ST} 55.2±10.3, active wakefulness 39.9±7.7; anesthetized 14.0±5.8; one-way RM ANOVA, state effect: F(2, 14)=28.3, p=1.2E-5; Figure 8D).

To test whether PCI^{ST} recovered to pre-anesthesia levels after anesthesia, we repeated the same set of 120 electrical stimuli up to two times over one hour following cessation of the isoflurane in a subset of mice. All but one subject showed an increase in PCI^{ST} in the first 30 minutes after cessation of isoflurane, but the complexity did not increase further in the subsequent 30 minutes (awake PCI^{ST} 48.0±4.0; anesthetized PCI^{ST} 14.3±2.3; recovery 0-30 minutes PCI^{ST} 32.7±4.9; recovery 30-60 minutes PCI^{ST} 36.4±5.0; RM ANOVA, state effect: F(3, 18)=11.6, p=1.8E-4; Figure 8E).

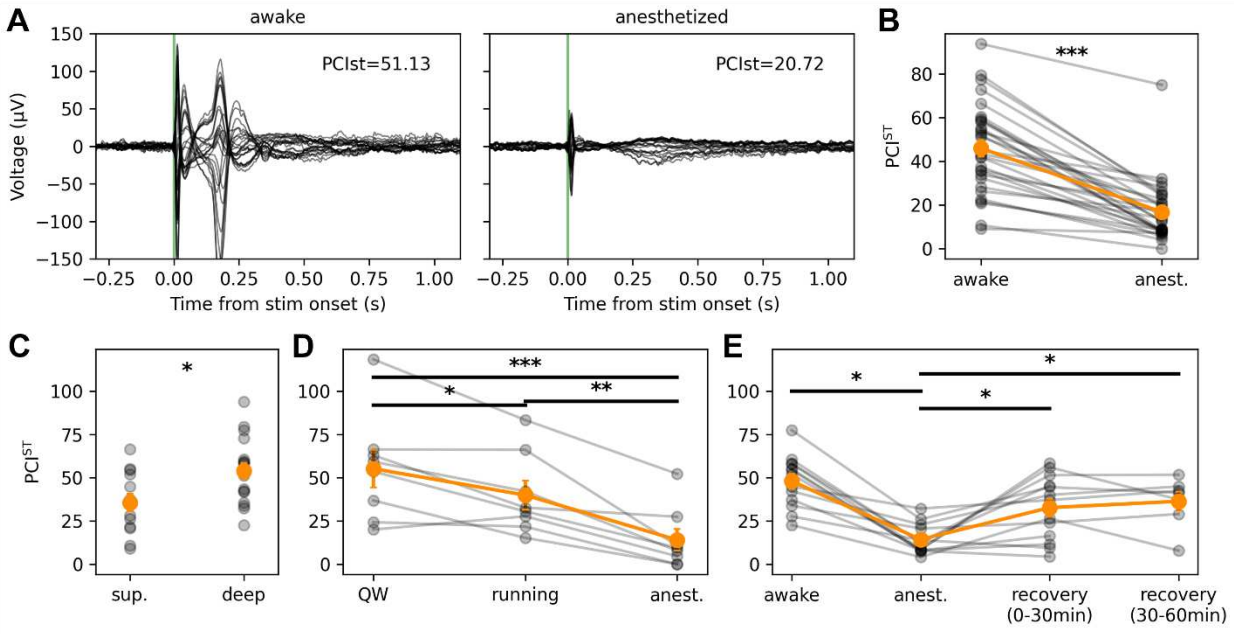

Figure 8: Perturbational complexity is modulated by CTC interactions.

(A) The ERP (-0.3 to +1.1 s) with all EEG electrode traces superimposed from the awake (left) and the anesthetized states (right). Same subject as in Figure 1D bottom left, annotated with PCI^{ST} values. **(B)** PCI^{ST} calculated using the EEG evoked responses (baseline -0.8 to -0.002 s and response 0.002 to 0.8 s) for the awake and anesthetized states. Individual values represented with gray connected circles (N=30 sessions across 23 mice). **(C)** PCI^{ST} for superficial versus deep cortical stimulation while mice are awake (includes quiet wakefulness and running trials). **(D)** PCI^{ST} for quiet wakefulness, running, and anesthetized states. Individual values represented with gray connected circles (N=8 mice). **(E)** PCI^{ST} for the quiet wakefulness, anesthetized, and two subsequent recovery states. Individual values represented with gray connected circles (N=13 mice). Orange circles and error bars represent mean ± SEM. * $p < 0.05$, ** $p < 0.01$, *** $p < 0.001$.

DISCUSSION

We record brain-wide, multi-scale, evoked EEG and Neuropixels responses to cortical electrical stimulation in head-fixed mice that are awake and, subsequently, anesthetized with isoflurane. We find that cortico-thalamo-cortical (CTC) interactions drive the long-lasting ERPs elicited by deep cortical stimulation during quiet wakefulness. Furthermore, the thalamic rebound response is characterized by thalamic burst firing that temporally coincides and is correlated with the second, late component in the ERP.

Stereotyped tri-phasic spiking pattern in cortical and thalamic neurons elicited by deep electrical stimulation

We observe a stereotyped, electrically-evoked spiking activity pattern – a brief excitation followed by 125.0±5.5 ms of inhibition – in local cortical neurons regardless of stimulation depth (superficial vs. deep), area (MO vs. SS), or behavioral state (quiet and active wakefulness, i.e., running, anesthetized). This pattern has been previously reported in different species (Butovas et al., 2006; Butovas & Schwarz, 2003; Chung & Ferster, 1998; Contreras & Steriade, 1995; Douglas & Martin, 1991; Grenier et al., 1998;

Hao et al., 2016; Kara et al., 2002; Logothetis et al., 2010; Sombeck et al., 2022; Vyazovskiy et al., 2013) and is reminiscent of the bi-stability reported in deep sleep and in unconscious patients following a brief stimulation (Hill & Tononi, 2005; Pigorini et al., 2015; Rosanova et al., 2018; Timofeev et al., 2001; Usami et al., 2015). Other studies also described rebound excitation at similar latencies following stimulation-evoked inhibitory periods (Butovas et al., 2006; Butovas & Schwarz, 2003; Grenier et al., 1998).

Given the direct projections from infragranular pyramidal neurons to thalamic regions (J. A. Harris et al., 2019; K. D. Harris & Shepherd, 2015; Hooks et al., 2013), it is not surprising that we observe strong recruitment of thalamic neurons 6.7 ms (on average) following the onset of cortical spiking. The thalamic spiking activity pattern evoked by deep stimulation during quiet wakefulness – brief excitation followed by a period of inhibition (74.6±15.5 ms) and a subsequent burst of action potentials – is consistent with previously described thalamic responses to cortical stimulation (Contreras & Steriade, 1995; Grenier et al., 1998). The fast action potential bursts we often observed in RS thalamic cells following the period of inhibition are likely to be triggered by low-threshold Ca^{2+} spikes, known to follow periods of pronounced hyperpolarization in thalamic relay neurons (Contreras & Steriade, 1995; Grenier et al., 1998; Guido & Weyand, 1995; Halassa et al., 2011; Lu et al., 1992; Nestvogel & McCormick, 2021; Urbain et al., 2019).

Evoked thalamic bursting consistently preceded cortical rebound spiking by 37.0 ms (on average, Figure 5F), comparable to the latency described by Grenier et al. (1998). This, together with their spike-width (> 0.4 ms; i.e., RS cells), is compatible with these being thalamic relay neurons that excite their cortical targets (Guo et al., 2017). Numerous previous studies have shown that thalamic relay neurons exhibit *spontaneous* bursting during anesthesia (Contreras & Steriade, 1995; Grenier et al., 1998; Swadlow & Gusev, 2001), NREM sleep (Halassa et al., 2011; Urbain et al., 2019), drowsiness (Stoelzel et al., 2009; Swadlow & Gusev, 2001), and wakefulness (Nestvogel & McCormick, 2021). Instead, our results show that thalamic relay neurons exhibit *evoked* rebound bursting during quiet wakefulness, but not during active wakefulness (i.*e.*, running*) or* isoflurane anesthesia. This is consistent with findings showing that thalamic hyperpolarization and low-threshold Ca^{2+} spike-bursting coincides with movement offset in mice (Nestvogel & McCormick, 2021). Likewise, some anesthetics decrease the probability of thalamic bursts; specifically, isoflurane has been shown to shunt the low-threshold Ca^{2+} spikes and, therefore, the associated bursting (Ries & Puil, 1999) (this does not rule out, of course, additional cortical sites of isoflurane; e.g., Bharioke et al., 2022). Therefore, our finding does not contradict results from other studies reporting evoked thalamic bursting in unconscious states, such as anesthesia via pentobarbital or ketamine/xylazine (Contreras & Steriade, 1995; Grenier et al., 1998) and NREM sleep (Urbain et al., 2019), which is likely to affect thalamic neurons in different ways compared to isoflurane.

Electrical stimulation evokes global ERP and LFP responses without associated wide-spread ipsilateral cortico-cortical spiking

Based on the presence of dense intracortical connections between areas (from neurons in layers 2/3-6; J. A. Harris et al., 2019), we expected that cortical stimulation during quiet wakefulness would elicit spiking elsewhere. However, we found little evidence of evoked spiking in ipsilateral non-stimulated cortical areas – ranging from stimulation-adjacent (0.5-1 mm away) to more than 5 mm away (Figure 3). Due to constraints on the experimental setup, we were unable to insert Neuropixels probes contralateral to the stimulated cortex. Current models suggest that the effects of microstimulation are predominantly mediated by activation of axons (Gustafsson & Jankowska, 1976; Hao et al., 2016; Histed

et al., 2009; Tehovnik et al., 2006). Because many axons project contralaterally, it is possible that the stimulation elicited cortical spiking contralaterally, as described by Vyazovskiy et al. (2013).

Yet even in the absence of evoked spiking in more distal cortical regions, we observe clear evoked activity in the LFP, in the form of significant, large-amplitude, evoked LFP fluctuations in cortical regions close by (0.5-1 mm) and up to 5 mm away (Figures 2 and 3). This finding is consistent with the contemporary understanding that LFP signals reflect presynaptic activity that may only weakly be driven by spiking (Herreras, 2016; Kajikawa & Schroeder, 2011; Łeski et al., 2013; Lindén et al., 2011). Our results show that the evoked LFP responses from distal cortical regions are not primarily due to local population spiking; we are unable, at present, to disentangle the possible contributions from presynaptic inputs or volume conduction. This modulation of the LFP signals is compatible with the wide-spread EEG signals we observe across the skull.

Thalamo-cortical dynamics modulate perturbational complexity in mice

The behavioral state of the mouse has strong effects on the underlying neural activity (Figure 7). Both running and anesthesia (isoflurane) modulate the excitability of the network, though in opposing directions. Thus, cortical firing rates during quiet wakefulness, 3.3±0.2 Hz, increase to 5.0±0.5 Hz for active wakefulness and decrease to 1.1±0.2 Hz during anesthesia (Figure 7E left); likewise in SM-TH, where baseline rates increase from 9.4±1.5 Hz during quiet wakefulness to 16.8±1.6 Hz during active wakefulness and drop to 0.8±0.4 Hz during anesthesia (Figure 7E right). Conversely, the median probability of electrically evoked thalamic bursting decreases from its baseline during quiet wakefulness of 9.5% ([10.0-23.7 IQR] to effectively zero for both active wakefulness [0-7.4 IQR] and anesthesia [0-0.2 IQR]).

Our findings suggest that stimulus-evoked bursts in the thalamus and the resulting thalamo-cortical interaction, that primarily occur when the animal is in quiet wakefulness, result in longer, higher amplitude ERPs (Figure 7C and 7D). This is consistent with previous studies showing that stimulus-evoked bursting in thalamic relay neurons robustly activates cortical neurons (Nestvogel & McCormick, 2021; Ramcharan et al., 2005; Stoelzel et al., 2009; Swadlow & Gusev, 2001), with a cortical rebound depolarization lasting up to ~0.5 s (Grenier et al., 1998), and 3-5 Hz cortical oscillation of ~1 s median duration (Nestvogel & McCormick, 2021). Indeed, the more thalamic cells burst during the rebound period, the larger the magnitude of the second, late component in the ERP (Figure S4). This observed link between the ERP and activity in the CTC loop is an important finding made possible by our unique experimental design.

ERPs are associated with higher PCI^{ST} values during awake than during anesthesia (quiet wakefulness PCI^{ST} 55.2±10.3; active wakefulness PCI^{ST} 39.9±7.7; anesthetized PCI^{ST} 14.0±5.8), consistent with prior work in humans (Comolatti et al., 2019) and in rats (Arena et al., 2021). Furthermore, the ERPs are shorter and the associated PCI^{ST} lower during active wakefulness than during quiet wakefulness (note that there are fewer running trials; for this comparison, trial numbers were matched within subject, on average 51 trials). Comolatti et al. (2019) showed that PCI^{ST} increased as the number of trials increased, specifically in wakefulness because averaging over more trials increases the signal-to-noise ratio of the ERP by reducing the contribution of background, non-stimulus-evoked activity. However, all subjects do have higher PCI^{ST} during active wakefulness compared to the anesthesia (active wakefulness PCI^{ST} 39.9±7.7; anesthetized PCI^{ST} 14.0±5.8). The comparison of PCI^{ST} across quiet wakefulness, active wakefulness, and anesthesia suggests that in mice there is an optimal network state which maximizes

complexity, reminiscent of the inverted-U relationship between arousal and task performance (McGinley et al., 2015; Yerkes & Dodson, 1908).

The last decade has witnessed the emergence of the mouse as a model organism to study the neuronal correlates of consciousness (Aru et al., 2020; Bharioke et al., 2022; Koch et al., 2016; Larkum, 2013; Sachidhanandam et al., 2013; Suzuki & Larkum, 2020). These studies point to the critical role of layer 5 pyramidal neurons, as well as cortico-cortical feedback to apical dendrites of infragranular pyramidal neurons. Although the present study was not designed with a classical perceived vs. non-perceived paradigm in mind (Koch et al., 2016), our finding of shorter and less complex ERPs and a reduced effectiveness of the CTC circuit during isoflurane anesthesia is certainly compatible with such results. To understand the extent to which our results generalize, it would be exciting to apply the PCI method to a diversity of different anesthesia in mice (e.g., Arena et al., 2021; Bharioke et al., 2022).

Limitations and benefits of studying ERPs in mice

There are qualitative differences between the ERPs we observed in mice and those in people (Casali et al., 2013; Comolatti et al., 2019; Ferrarelli et al., 2010; Massimini et al., 2005): most importantly, the two robust components (at 25 and 180 ms post-stimulation) in the ERPs from mice in quiet wakefulness are not apparent in human TMS-evoked EEG. Of course, there are several key differences between the brains of these two species, the most important being the three orders of magnitude difference in volume and number of neurons. The mouse brain is roughly 0.5 cm^3 and contains 71 million neurons whereas the human brain is closer to 1200 cm^3 with 86 billion neurons (Herculano-Houzel et al., 2006; von Bartheld et al., 2016; Walløe et al., 2014). The smooth mouse neocortex is 0.8-1 mm thick, with 14 million neurons whereas the highly folded human neocortex is 2.5-3.0 mm thick with 16 billion neurons (Herculano-Houzel et al., 2006; Walløe et al., 2014).

Another possible explanation for the striking difference in the ERPs is the different biophysical modes of stimulation – direct current flow from and to the inserted electrode versus a magnetic-field induced current flow in the cortical tissue underneath the TMS coil resting against the scalp. Electrical stimulation leads to direct activation of local cells and axons that run near the stimulation site via activation of the axon initial segment (Gustafsson & Jankowska, 1976; Histed et al., 2009; Sombeck et al., 2022; Tehovnik et al., 2006; Terao & Ugawa, 2002), whereas TMS elicits indirect waves of cortical activation by exciting axons and neurons mainly trans-synaptically (Pashut et al., 2014; Siebner et al., 2022; Terao & Ugawa, 2002).

Despite these differences, this study led to novel and unexpected results linking the ERP to activity in the CTC loop. There are many additional open questions regarding neural mechanisms underlying spontaneous and stimulus-evoked EEG signals (Cohen, 2017). Rodent models offer a unique opportunity to combine EEG recordings with high-density extracellular recording technology to shine light on the underlying microcircuit dynamics. This study opens the door for future work with rodents using different perturbational techniques (e.g., chemogenetics, optogenetics, TMS [Senda et al., 2021]) to causally link the contributions of different cell types, brain regions, and network dynamics to EEG signals and ERP features commonly used in clinical and research settings.

ACKNOWLEDGEMENTS

We thank Anton Arkhipov, Matias Cavelli, Chiara Cirelli, Graham Findlay, Saurabh Gandhi, Soo Yeun Lee, Rong Mao, Marcello Massimini, Dana Mastrovito, Ethan McBride, David McCormick, Stefan Mihalas,

Andrea Pigorini, Simone Russo, Simone Sarasso, and Giulio Tononi for helpful discussions and intellectual contributions.

We thank the Animal Care and Lab Animal Services teams for mouse husbandry and care and the Manufacturing and Process Engineering team for experimental hardware and software support. We gratefully acknowledge funding from the Tiny Blue Dot Foundation for this study. We thank the Allen Institute founder, Paul G. Allen, for his vision, encouragement, and support.

AUTHOR CONTRIBUTIONS

Conceptualization and Methodology, L.D.C., I.R., S.R.O., and C.K.; Formal Analysis, L.D.C. and I.R.; Investigation, L.D.C., I.R., J.R.K., and L.C.M.; Data Curation, L.D.C., I.R., J.R.K., and L.C.M.; Writing – Original Draft, L.D.C., I.R., and C.K.; Writing – Review & Editing, L.D.C., I.R., J.R.K., L.C.M., S.R.O., and C.K.; Visualization, L.D.C.; Supervision, S.R.O. and C.K.; Funding Acquisition, C.K.

DECLARATION OF INTERESTS

The authors declare no competing interests.

METHODS

Experimental procedures closely followed those described in Siegle, Jia et al. (2021). A summary of these methods and details of procedures that differ are provided below.

Mice

Mice were maintained in the Allen Institute animal facility and used in accordance with protocols approved by the Allen Institute's Institutional Animal Care and Use Committee. All experiments used C57BL/6J wild-type mice (N = 37). Male and female wild-type C57BL/6J mice were purchased from Jackson Laboratories at postnatal day 28 and they were 9-28 weeks old at the time of all *in vivo* electrophysiological recordings.

After surgery, all mice were single-housed and maintained on a reverse 12-h light cycle in a shared facility with room temperatures between 20 and 22 °C and humidity between 30 and 70%. All experiments were performed during the dark cycle. Mice had ad libitum access to food and water.

Surgical procedures and habituation

Each mouse went through the following order of procedures prior to the day of the experiment: 1) an initial sterile surgery to implant an EEG array and a titanium headframe for head-fixed electrophysiological experiments *in vivo*; 2) five days of recovery time post-surgery; 3) at least three weeks of habituation to head-fixation; 4) and a second sterile surgery to perform small craniotomies to allow for insertion of the stimulating electrode and Neuropixels probes.

One to three hours prior to each surgery, pre-operative injections of dexamethasone (3-4 mg/kg, IM) and ceftriaxone (100-125 mg/kg, SC) were administered. Mice were deeply anesthetized with isoflurane (5% isoflurane induction, 1.5-2.5% maintenance) and placed in a stereotaxic frame. Vital signs were monitored, body temperature was maintained at 37.5 °C with a heating pad under the animal (TC-1000 temperature controller, CWE, Inc.), and ocular lubricant (I Drop, VetPLUS) was applied to maintain hydration of the eyes during anesthesia. Atropine (0.02-0.05 mg/kg, SC) and carprofen (5-10 mg/kg, SC) were administered at the start of the procedure. After the surgical procedure, mice received an injection of lactated Ringer's solution (up to 1 mL, SC) and recovered on a heating pad. Animals received two days of analgesics and antibiotics post-surgery.

The initial surgery was performed on healthy mice that ranged in age from 5-20 weeks. Mice were deeply anesthetized prior to removing skin and exposing the skull. After leveling the skull, a 30-electrode mouse EEG array (NeuroNexus Technologies, Inc., Ann Arbor, Michigan) was carefully positioned on top of the skull and fixed in place with Kwik-Cast (World Precision Instruments, Inc., Sarasota, Florida). Skull screws were implanted either over the right olfactory bulb or left and right cerebellum that functioned as reference and ground for the EEG signals. White C&B Metabond (Parkell, Inc., Edgewood, New York) was then used to secure a custom titanium headframe and the EEG array to the skull. After five days of recovery, mice spent at least three weeks being habituated to handling and head-fixation.

Following habituation and up to one day before the recording, mice underwent the second surgical procedure. Under a microscope, the skull was exposed by drilling through the outer layer of Metabond then removing the Kwik-Cast and a small portion of the EEG polymer substrate, carefully avoiding damage to the EEG contacts. Up to three small craniotomies (less than 0.5 mm in diameter) were drilled to allow access to the brain regions of interest for the subsequent experiment. A small piece of artificial cerebrospinal fluid (**ACSF**)-soaked gel-foam sponge was positioned on top of each craniotomy and Kwik-

Cast was used to seal it. A 3D-printed plastic well was also fixed to the existing Metabond around the craniotomies.

In-vivo recording and stimulation

The day of the experiment, the mouse was placed on the running wheel and fixed to the headframe clamp with two set screws. Next, the thin layer of Kwik-Cast was removed to expose the craniotomies and abundant ACSF was added on top of the skull to prevent the exposed brain tissue from drying out. A 3D-printed cone was lowered to prevent the mouse's tail from contacting the probes and a black curtain was lowered over the front of the rig, placing the mouse in complete darkness.

EEG recording

All 30 EEG electrodes were connected to a 32-channel head-stage (RHD 32ch, Intan Technologies, Los Angeles, California) controlled by an Open Ephys acquisition board (Siegle et al., 2017). EEG signals were sampled at 2.5 kHz with a low-frequency cutoff of 0.1 Hz and digitized with 16-bit resolution. Each circular, platinum electrode on the EEG array had a diameter of 500 µm and an impedance of 0.01 MΩ (impedance measured by the manufacturer). All subjects had a skull screw implanted over the right cerebellum (penetrating the skull but not the dura) that served as electrical ground. One of the following served as a common refence electrode for the EEG signals: a 0.7 x 0.7 mm square platinum surface electrode above the left cerebellum, a skull screw implanted over the right olfactory bulb, or a skull screw implanted over the left cerebellum.

Neuropixels recording

In a subset of mice (N=26/37), simultaneous recordings from the EEG array and multiple Neuropixels probes (Jun et al., 2017) were performed. These experiments used Neuropixels 3a prototypes or standard Neuropixels 1.0 probes configured to record from the 384 electrodes closest to the tip of the probe. The signals from each recording site were split in hardware into a spike band (30 kHz sampling rate, 500 Hz high-pass filter, 500x gain) and an LFP band (2.5 kHz sampling rate, 1,000 Hz low-pass filter, 250x gain) and data was acquired using the Open Ephys GUI (Siegle et al., 2017). Each probe was either connected to a dedicated FPGA streaming data over Ethernet (Neuropixels 3a) or a PXIe card inside a National Instruments chassis (Neuropixels 1.0).

The reference connection on the Neuropixels probes was permanently soldered to ground using a silver wire, and all recordings were made using either an external reference configuration (Neuropixels 3a) or a tip reference configuration (Neuropixels 1.0). All Neuropixels head-stage grounds, which were contiguous with the probe grounds, were connected in parallel to animal ground – a 32 AWG silver wire (A-M Systems) placed in the ACSF on top of the craniotomies.

Neuropixels insertion

During the acute electrophysiological experiment, up to three Neuropixels probes were inserted targeting motor (MO), anterior cingulate (ACA), somatosensory (SS), visual (VIS), and thalamic nuclei. We restricted our analysis of thalamic nuclei to those that had strong projections to and/or from motor and somatosensory areas (Guo et al., 2017; J. A. Harris et al., 2019): anteroventral (AV), central lateral (CL), mediodorsal (MD), posterior (PO), reticular (RT), ventral anterior-lateral (VAL), ventral posterolateral (VPL), ventral posteromedial (VPM), and ventral medial (VM). We refer to these collectively as the somatomotor-related thalamic nuclei (SM-TH), disregarding the distinction between first and higher order thalamic regions.

The probe insertion process followed the steps detailed by Siegle, Jia et al. (2021). Briefly, each probe was individually inserted into the brain using a 3-axis micromanipulator (New Scale Technologies, Victor, New York) at a rate of 200 µm per min to a depth of 3.5 mm or less in the brain. After the probes reached their targets, they were allowed to settle for 10-15 min before starting the experiment. Before insertion, all Neuropixels probes were coated with a fluorescent dye (Vybrant DiI/DiO/DiD, ThermoFisher Scientific, Waltham, Massachusetts) by repeatedly immersing them in a well filled with the dye and removing each probe slowly allowing the dye to dry on the surface.

Behavioral data and synchronization

The angular position of the running wheel and the synchronization signal for the electrical stimulus were acquired by a dedicated computer with a National Instruments card acquiring digital inputs at 100 kHz, which was considered the master clock. A 32-bit digital "barcode" was sent with an Arduino Uno (SparkFun DEV-11021) every 30 s to synchronize all devices with the neural data from the EEG array and the Neuropixels probes. Details regarding the post-hoc data synchronization using the barcodes are described by Siegle, Jia et al. (2021).

Cortical Stimulation

Electrical stimulation was delivered through a custom bipolar platinum-iridium stereotrode (Microprobes for Life Science, Gaithersburg, Maryland) consisting of two parallel monopolar electrodes (50 kOhm impedance) with a vertical offset of 300 µm between the two tips. During each stage of the experiment, up to 120 biphasic, charge-balanced, cathodic-first current pulses (200 µs per phase, 3.5-4.5 s inter-stimulus interval) were delivered at three different current intensities (360 pulses total). The current intensities were chosen for each animal while it was awake before starting the experiment based on the following criteria: 1) the electrical pulse did not evoke any visible twitches and 2) the medium current elicited visible averaged evoked responses for most of the EEG electrodes ($n > 15$) defined as 3 standard deviations above baseline for at least 100 ms following the stimulus onset.

The stimulation electrode was acutely inserted using a 3-axis micromanipulator, like the Neuropixels probes. We targeted four locations for stimulation: secondary motor cortex (MOs), layer 2/3 (N=10 mice, 0.37±0.04 mm below the brain surface); MOs, layer 5/6 (N=11 mice, 1.15±0.06 mm below the brain surface); primary somatosensory cortex (SSp), layer 2/3 (N=8 mice, 0.47±0.06 mm below the brain surface); and SSp, layer 5/6 (N=11 mice, 0.92±0.05 mm below the brain surface). Some mice received stimulation in multiple locations (N=10). Before insertion, the stimulation electrode was coated with a fluorescent dye, like the Neuropixels probes.

Experimental timeline

The paired EEG/Neuropixels recordings were acute, lasting 2-3 hours. At the beginning, awake head-fixed mice (free to run on or rest on the running wheel) were exposed to electrical stimuli after 5 min of baseline recording without stimulation. After the awake session, mice were anesthetized via inhaled isoflurane (5% induction) delivered through a small tube placed in front of the mouse's nose. Once a surgical level of anesthesia was reached, the animal was maintained unconscious by keeping the isoflurane level at 1-1.5%. The unconscious state was verified by lack of reaction to noxious stimuli such as toe or tail pinch and alcohol pad close to the nose of the animal. The EEG signals were also continuously monitored to avoid the burst suppression mode indicative of very deep anesthesia (Purdon et al., 2015). Then the same electrical stimuli session was repeated. While under anesthesia, we recorded the precise concentration of isoflurane delivered over time, in addition to the data streams

listed above. Finally, the isoflurane was turned off and the mouse recovered. In a subset of mice (N=16), the electrical stimuli were delivered for a third (and sometimes a fourth) time during the recovery period. The resulting dataset allowed a direct comparison of the evoked neural responses across different brain states (quiet wakefulness, running, anesthetized, recovery).

Probe removal and cleaning

Upon completion of the experiment, probes were retracted from the brain at a rate of 1 mm/s. The craniotomies were protected with a small piece of ACSF-soaked gel-foam sponge and a thin layer of Kwik-Cast before mice were removed from head fixation and returned to their home cages overnight. The probes and the stimulating electrode were immersed in a well of 1% Tergazyme for around 2-6 h to remove residual tissue, and then rinsed in purified water.

Quality control for the EEG experiments

Overall EEG signal quality

Before the experiment, the EEG signals were tested by exposing the animal to visual flashes and evaluating the signal-to-noise ratio of the EEG evoked responses. Animals with low signal-to-noise ratio, high levels of 60 Hz noise, or large movement artifacts were not used for the experiment (8 mice).

EEG stimulation artifact

If more than half of the EEG channels over the course of the experiment showed large stimulation artifacts lasting for hundreds of milliseconds after the stimulation onset, the session was excluded (8 sessions across 6 mice). In total, out of 37 implanted mice, 23 were included in the study.

Ex vivo imaging and localization of electrodes

After the experiment, mice were deeply anesthetized (5% isoflurane) and perfused with 4% paraformaldehyde. The brains were preserved in 4% paraformaldehyde for 48 hours, rinsed with 1x PBS, and stored at 4 °C in PBS. The brains were then processed in one of two ways: brains were sliced into 100 µm coronal sections using a vibratome (Leica VT1000S) and imaged with a fluorescent microscope (Olympus VS110/120) at 10x magnification or whole brains were imaged using serial two-photon tomography (Oh et al., 2014; Ragan et al., 2012).

Images of the 100 µm coronal sections were aligned to the Allen Institute Common Coordinate Framework (CCFv3) following the process detailed by McBride et al. (2022) and images from serial two-photon tomography were aligned to the CCFv3 following the process detailed by Oh et al. (2014). Fluorescent tracks corresponding to the location of the Neuropixels probes and the stimulation electrode were manually identified in the aligned images. Because each CCFv3 coordinate corresponds to a unique brain region, the precision of brain region assignments is determined by the resolution of the CCFv3, which was 25 µm per pixel. For each Neuropixels probe the locations of major structural boundaries along the track was manually aligned with the physiology data (Liu et al., 2021; Siegle et al., 2021). Then each recording channel along the Neuropixels probe (and associated neurons) was assigned to a unique CCFv3 structure. Other studies have reported better than 0.1 mm accuracy for electrode localization following similar methods (Liu et al., 2021).

Data processing

Stimulus artifact masking

In all recordings we observed short latency voltage transients time-locked to the stimulus. Though the stimulus had a total duration of 0.4 ms, artifacts sometimes lasted up to 2 ms. To mask the artifact, the

raw signal from -2 to 0 ms was copied, reversed, and replaced the 0 to 2 ms artifact window. The same masking procedure was used across all electrophysiology data types.

EEG

After artifact masking, EEG recordings were visually inspected to identify electrodes containing noise artifacts or remaining large and long stimulation artifacts. These were excluded from further analysis, leaving an average of 23 +/- 4 artifact-free electrodes out of 30 for each subject. EEG signals from all good electrodes were re-referenced to the common average across electrodes and bandpass filtered from 0.1 to 100 Hz (Butterworth filter, 3rd order). Finally, the continuous EEG signals were segmented into epochs from -2 to +2 s from stimulus onset and saved for further analysis.

Neuropixels LFP

After artifact masking, LFP signals were down sampled from 2.5 kHz to 1.25 kHz after applying an anti-aliasing filter. The signals were then high pass filtered (Butterworth filter, 1st order) and re-referenced to the median signal from electrodes that were in the ACSF above the brain surface (to remove common signal from the tip reference electrode). Finally, the continuous LFP signals were segmented into epochs from -2 to +2 s from stimulus onset and saved for further analysis.

Spike sorting

After applying the artifact masking to the raw spike band data, it was pre-processed and spike-sorted using Kilosort 2.0 (Stringer et al., 2019) as described by Siegle, Jia et al. (2021). After spike sorting, any spikes that occurred during the artifact window (0 to +2 ms from stimulus onset) were removed from further analysis. High quality units were identified for further analysis using metrics described by Siegle, Jia et al. (2021).

Data Analysis

EEG event-related potentials (ERPs)

Across each experiment, trials were classified by the behavioral state of the animal: quiet wakefulness, if the mouse's speed (measured by the wheel's angular velocity) was equal to 0 cm/s from -0.5 to +0.5 s from the stimulus onset; running, if the mouse's speed was greater than 0 cm/s; anesthetized, when the mouse was unconscious; and recovery, after the isoflurane delivery was discontinued. ERPs associated with a given state were then compiled by averaging all EEG traces assigned to that state.

ERP magnitude and duration

To quantify the ERP metrics, the trial-averaged EEG signals (-2 to +2 s after stimulus onset) were used to calculate the global field power (global mean field power) by taking the standard deviation across all channels for every time point (Cohen, 2014; Esser et al., 2006; Lehmann & Skrandies, 1980). Next, the z-score of the global field power was computed relative to baseline values (-2 to 0 s). The duration of the response was measured as the length of time the global field power (z-score) was greater than three standard deviations above baseline (z=3) in the response window (0 to +2 s). The magnitude of the response was calculated by integrating under the global field power (z-score) but above z=3 in the response window and dividing it by the area under the baseline window (see Figure S2).

LFP and population spiking magnitude

To quantify the magnitude of the evoked LFP response, the spatial average of the rectified, trial averaged LFP signal for all channels in the respective cortical region, all layers except for layer 1. Then the area under the curve was calculated for the post-stimulus period (0 to +2 s) of the global field power

(z-score of the baseline) and divided by area under the curve of the baseline (-2 to 0 s). A similar procedure was used for the population spiking, except the signals used were single neuron spike density functions. For both data types, the significance of the response was determined using the two-sample Kolmogorov-Smirnov test (p-values less than 0.01 were considered significant) to compare the underlying distributions of the baseline (-2 to 0 s) and the response (0 to +2 s) values.

Significantly modulated neurons

The fraction of neurons modulated by the electrical stimulation was quantified following the method detailed by McBride et al. (2022). Briefly, for each neuron pre- and post-stimulus spikes were counted on a trial-by-trial basis for the specified windows: 2-25 ms, 25-150 ms, and 150-300 ms. The duration of the window was always matched for pre- and post-stimulus. Then a Wilcoxon sign-rank test was performed on the trial-wise pre- and post-stimulus spike counts to obtain a p-value. The p-values obtained for all RS neurons in all areas of interest were corrected using the Benjamini-Hochberg correction with the false discovery rate set at 0.01. Neurons with an adjusted p-value < 0.01 were considered significantly modulated. They were labeled as “increased” or “decreased” based on whether their spike count increased or decreased, respectively, in the post-stimulus window relative to the pre-stimulus window on average.

Perturbational Complexity Index, state-transition (PCI^{ST})

PCI^{ST} was used to evaluate the spatiotemporal complexity of the EEG ERPs for each brain state (Comolatti et al., 2019). PCI^{ST} was computed using the code available at github.com/renzocom/PCIst and the parameters were set as follows: baseline window = [-0.8, -0.002] s; response window = [0.002, 0.8] s; minimum SNR = 1.6; maximum variance = 99%; and the parameter k = 1.2. In all calculations, the number of trials per state within subject was matched.

Statistics

Statistical analysis was performed in Python. All data was tested for normality using the Shapiro-Wilk test from the SciPy package (scipy.stats.shapiro). For normally distributed datasets we used the unpaired t-test (scipy.stats.ttest_ind) or the paired t-test (scipy.stats.ttest_rel). For non-parametric datasets we used the Mann-Whitney U test (scipy.stats.mannwhitneyu) or the Wilcoxon signed-rank test (scipy.stats.wilcoxon). All comparisons using t-tests are two-sided. Statistical comparisons between multiple groups were performed using both parametric (ANOVA) and non-parametric (Friedman) tests with post hoc, pairwise comparisons corrected for multiple comparisons. Correlational analyses were performed using Pearson correlation coefficients.

In all figures, the convention is * $p < 0.05$, ** $p < 0.01$, *** $p < 0.001$. The values in the text indicate the mean and standard error of the mean (mean ± SEM) or the median and IQR [25^{th} and 75^{th} percentiles] for normally distributed and non-parametric datasets, respectively.

REFERENCES

Arena, A., Comolatti, R., Thon, S., Casali, A. G., & Storm, J. F. (2021). General Anesthesia Disrupts Complex Cortical Dynamics in Response to Intracranial Electrical Stimulation in Rats. *ENeuro*, *8*(4). https://doi.org/10.1523/ENEURO.0343-20.2021

Aru, J., Suzuki, M., & Larkum, M. E. (2020). Cellular Mechanisms of Conscious Processing. *Trends in Cognitive Sciences*, *24*(10), 814–825. https://doi.org/10.1016/j.tics.2020.07.006

Bai, Y., Lin, Y., & Ziemann, U. (2021). Managing disorders of consciousness: the role of electroencephalography. In *Journal of Neurology* (Issue 268). Springer Berlin Heidelberg. https://doi.org/10.1007/s00415-020-10095-z

Bai, Y., Xia, X., & Li, X. (2017). A review of resting-state electroencephalography analysis in disorders of consciousness. *Frontiers in Neurology*, *8*(SEP), 471. https://doi.org/10.3389/FNEUR.2017.00471

Bharioke, A., Munz, M., Brignall, A., Kosche, G., Eizinger, M. F., Ledergerber, N., Hillier, D., Gross-Scherf, B., Conzelmann, K.-K., Macé, E., & Roska, B. (2022). General anesthesia globally synchronizes activity selectively in layer 5 cortical pyramidal neurons. *Neuron*, *0*(0). https://doi.org/10.1016/J.NEURON.2022.03.032

Butovas, S., Hormuzdi, S. G., Monyer, H., & Schwarz, C. (2006). Effects of electrically coupled inhibitory networks on local neuronal responses to intracortical microstimulation. *Journal of Neurophysiology*, *96*(3), 1227–1236. https://doi.org/10.1152/jn.01170.2005

Butovas, S., & Schwarz, C. (2003). Spatiotemporal Effects of Microstimulation in Rat Neocortex: A Parametric Study Using Multielectrode Recordings. *Journal of Neurophysiology*, *90*, 3024–3039. https://doi.org/10.1152/jn.00245.2003

Casali, A. G., Gosseries, O., Rosanova, M., Boly, M., Sarasso, S., Casali, K. R., Casarotto, S., Bruno, M. A., Laureys, S., Tononi, G., & Massimini, M. (2013). A theoretically based index of consciousness independent of sensory processing and behavior. *Science Translational Medicine*, *5*(198). https://doi.org/10.1126/scitranslmed.3006294

Casarotto, S., Comanducci, A., Rosanova, M., Sarasso, S., Fecchio, M., Napolitani, M., Pigorini, A., Casali, A. G., Trimarchi, P. D., Boly, M., Gosseries, O., Bodart, O., Curto, F., Landi, C., Mariotti, M., Devalle, G., Laureys, S., Tononi, G., & Massimini, M. (2016). Stratification of Unresponsive Patients by an Independently Validated Index of Brain Complexity. *Annals of Neurology*, *80*(5), 718–729. https://doi.org/10.1002/ana.24779

Chung, S., & Ferster, D. (1998). Strength and orientation tuning of the thalamic input to simple cells revealed by electrically evoked cortical suppression. *Neuron*, *20*(6), 1177–1189. https://doi.org/10.1016/S0896-6273(00)80498-5

Claudi, F., Tyson, A. L., Petrucco, L., Margrie, T. W., Portugues, R., & Branco, T. (2021). Visualizing anatomically registered data with brainrender. *ELife*, *10*. https://doi.org/10.7554/ELIFE.65751

Cohen, M. X. (2014). Analyzing Neural Time Series Data: Theory and Practice. In *Analyzing Neural Time Series Data*. The MIT Press. https://doi.org/10.7551/MITPRESS/9609.001.0001

Cohen, M. X. (2017). Where Does EEG Come From and What Does It Mean? *Trends in Neurosciences*, *40*(4), 208–218. https://doi.org/10.1016/j.tins.2017.02.004

Comolatti, R., Pigorini, A., Casarotto, S., Fecchio, M., Faria, G., Sarasso, S., Rosanova, M., Gosseries, O.,

Boly, M., Bodart, O., Ledoux, D., Brichant, J.-F., Nobili, L., Laureys, S., Tononi, G., Massimini, M., & Casali, A. G. (2019). A fast and general method to empirically estimate the complexity of brain responses to transcranial and intracranial stimulations. *Brain Stimulation*. https://doi.org/10.1016/J.BRS.2019.05.013

Contreras, D., & Steriade, M. (1995). Cellular Basis of EEG Slow Rhythms: A Study of Dynamic Corticothalamic Relationships. *The Journal of Neuroscience*, *15*(1), 604–622. https://doi.org/10.1523/JNEUROSCI.15-01-00604.1995

D'Andola, M., Rebollo, B., Casali, A. G., Weinert, J. F., Pigorini, A., Villa, R., Massimini, M., & Sanchez-Vives, M. V. (2018). Bistability, Causality, and Complexity in Cortical Networks: An In Vitro Perturbational Study. *Cerebral Cortex*, *28*(7), 2233–2242. https://doi.org/10.1093/cercor/bhx122

Dasilva, M., Camassa, A., Navarro-Guzman, A., Pazienti, A., Perez-Mendez, L., Zamora-López, G., Mattia, M., & Sanchez-Vives, M. V. (2021). Modulation of cortical slow oscillations and complexity across anesthesia levels. *NeuroImage*, *224*, 117415. https://doi.org/10.1016/j.neuroimage.2020.117415

Douglas, R. J., & Martin, K. A. C. (1991). A Functional Microcircuit for Cat Visual Cortex. *Journal of Physiology*, *440*, 735–769. https://doi.org/10.1113/jphysiol.1991.sp018733

Esser, S. K., Huber, R., Massimini, M., Peterson, M. J., Ferrarelli, F., & Tononi, G. (2006). A direct demonstration of cortical LTP in humans: A combined TMS/EEG study. *Brain Research Bulletin*, *69*(1), 86–94. https://doi.org/10.1016/J.BRAINRESBULL.2005.11.003

Farisco, M., Pennartz, C., Annen, J., Cecconi, B., & Evers, K. (2022). Indicators and criteria of consciousness: ethical implications for the care of behaviorally unresponsive patients. *BMC Medical Ethics*, *23*. https://doi.org/10.1186/s12910-022-00770-3

Ferrarelli, F., Massimini, M., Sarasso, S., Casali, A., Riedner, B. A., Angelini, G., Tononi, G., & Pearce, R. A. (2010). Breakdown in cortical effective connectivity during midazolam-induced loss of consciousness. *Proceedings of the National Academy of Sciences of the United States of America*, *107*(6), 2681–2686. https://doi.org/10.1073/pnas.0913008107

Frohlich, J., Toker, D., & Monti, M. M. (2021). Consciousness among delta waves: A paradox? *Brain*, *144*(8), 2257–2277. https://doi.org/10.1093/brain/awab095

Grenier, F., Timofeev, I., & Steriade, M. (1998). Leading role of thalamic over cortical neurons during postinhibitory rebound excitation. *Proceedings of the National Academy of Sciences of the United States of America*, *95*(23), 13929–13934. https://doi.org/10.1073/pnas.95.23.13929

Guido, W., & Weyand, T. (1995). Burst responses in thalamic relay cells of the awake behaving cat. *Journal of Neurophysiology*, *74*(4), 1782–1786. https://doi.org/10.1152/JN.1995.74.4.1782

Guo, Z. V., Inagaki, H. K., Daie, K., Druckmann, S., Gerfen, C. R., & Svoboda, K. (2017). Maintenance of persistent activity in a frontal thalamocortical loop. *Nature*, *545*(7653), 181–186. https://doi.org/10.1038/nature22324

Gustafsson, B., & Jankowska, E. (1976). Direct and Indirect Activation of Nerve Cells by Electrical Pulses Applied Extracellularly. *Journal of Physiology*, *258*, 33–61. https://doi.org/10.1113/jphysiol.1976.sp011405

Halassa, M. M., Siegle, J. H., Ritt, J. T., Ting, J. T., Feng, G., & Moore, C. I. (2011). Selective optical drive of thalamic reticular nucleus generates thalamic bursts and cortical spindles. *Nature Neuroscience*,

14(9), 1118–1120. https://doi.org/10.1038/nn.2880

Hao, Y., Riehle, A., & Brochier, T. G. (2016). Mapping horizontal spread of activity in monkey motor cortex using single pulse microstimulation. *Frontiers in Neural Circuits*, *10*(DEC), 104. https://doi.org/10.3389/FNCIR.2016.00104

Harris, J. A., Mihalas, S., Hirokawa, K. E., Whitesell, J. D., Choi, H., Bernard, A., Bohn, P., Caldejon, S., Casal, L., Cho, A., Feiner, A., Feng, D., Gaudreault, N., Gerfen, C. R., Graddis, N., Groblewski, P. A., Henry, A. M., Ho, A., Howard, R., … Zeng, H. (2019). Hierarchical organization of cortical and thalamic connectivity. *Nature*, *575*. https://doi.org/10.1038/s41586-019-1716-z

Harris, K. D., & Shepherd, G. M. G. (2015). The neocortical circuit: Themes and variations. *Nature Neuroscience*, *18*(2), 170–181. https://doi.org/10.1038/nn.3917

Herculano-Houzel, S., Mota, B., & Lent, R. (2006). Cellular scaling rules for rodent brains. *Proceedings of the National Academy of Sciences of the United States of America*, *103*(32), 12138–12143. https://doi.org/10.1073/PNAS.0604911103

Herreras, O. (2016). Local field potentials: Myths and misunderstandings. *Frontiers in Neural Circuits*, *10*(DEC), 101. https://doi.org/10.3389/FNCIR.2016.00101

Hill, S., & Tononi, G. (2005). Modeling sleep and wakefulness in the thalamocortical system. *Journal of Neurophysiology*, *93*(3), 1671–1698. https://doi.org/10.1152/JN.00915.2004

Histed, M. H., Bonin, V., & Reid, R. C. (2009). Direct Activation of Sparse, Distributed Populations of Cortical Neurons by Electrical Microstimulation. *Neuron*, *63*(4), 508–522. https://doi.org/10.1016/j.neuron.2009.07.016

Hooks, B. M., Mao, T., Gutnisky, D. A., Yamawaki, N., Svoboda, K., & Shepherd, G. M. G. (2013). Organization of Cortical and Thalamic Input to Pyramidal Neurons in Mouse Motor Cortex. *The Journal of Neuroscience*, *33*(2), 748–760. https://doi.org/10.1523/JNEUROSCI.4338-12.2013

Jonak, C. R., Lovelace, J. W., Ethell, I. M., Razak, K. A., & Binder, D. K. (2018). Reusable Multielectrode Array Technique for Electroencephalography in Awake Freely Moving Mice. *Frontiers in Integrative Neuroscience*, *12*, 53. https://doi.org/10.3389/fnint.2018.00053

Jun, J. J., Steinmetz, N. A., Siegle, J. H., Denman, D. J., Bauza, M., Barbarits, B., Lee, A. K., Anastassiou, C. A., Andrei, A., Aydin, Ç., Barbic, M., Blanche, T. J., Bonin, V., Couto, J., Dutta, B., Gratiy, S. L., Gutnisky, D. A., Häusser, M., Karsh, B., … Harris, T. D. (2017). Fully integrated silicon probes for high-density recording of neural activity. *Nature*, *551*(7679), 232–236. https://doi.org/10.1038/nature24636

Kajikawa, Y., & Schroeder, C. E. (2011). How local is the local field potential? *Neuron*, *72*(5), 847–858. https://doi.org/10.1016/J.NEURON.2011.09.029

Kara, P., Pezaris, J. S., Yurgenson, S., & Reid, R. C. (2002). The spatial receptive field of thalamic inputs to single cortical simple cells revealed by the interaction of visual and electrical stimulation. *Proceedings of the National Academy of Sciences of the United States of America*, *99*(25), 16261–16266. https://doi.org/10.1073/pnas.242625499

Kobylarz, E. J., & Schiff, N. D. (2005). Neurophysiological correlates of persistent vegetative and minimally conscious states. *Neuropsychological Rehabilitation*, *15*, 323–332. https://doi.org/10.1080/09602010443000605

Koch, C., Massimini, M., Boly, M., & Tononi, G. (2016). Neural correlates of consciousness: progress and problems. *Nature Reviews Neuroscience*, *17*, 307–321. https://doi.org/10.1038/nrn.2016.22

Land, R., Kapche, A., Ebbers, L., & Kral, A. (2019). 32-channel mouse EEG: Visual evoked potentials. *Journal of Neuroscience Methods*, 108316. https://doi.org/10.1016/j.jneumeth.2019.108316

Larkum, M. (2013). A cellular mechanism for cortical associations: an organizing principle for the cerebral cortex. *Trends in Neurosciences*, *36*(3), 141–151. https://doi.org/10.1016/J.TINS.2012.11.006

Lehmann, D., & Skrandies, W. (1980). Reference-free identification of components of checkerboard-evoked multichannel potential fields. *Electroencephalography and Clinical Neurophysiology*, *48*(6), 609–621. https://doi.org/10.1016/0013-4694(80)90419-8

Łeski, S., Lindé, H., Tetzlaff, T., Pettersen, K. H., & Einevoll, G. T. (2013). Frequency Dependence of Signal Power and Spatial Reach of the Local Field Potential. *PLoS Computational Biology*, *9*(7), e1003137. https://doi.org/10.1371/journal.pcbi.1003137

Lindén, H., Tetzlaff, T., Potjans, T. C., Pettersen, K. H., Grü, S., Diesmann, M., & Einevoll, G. T. (2011). Modeling the Spatial Reach of the LFP. *Neuron*, *72*, 859–872. https://doi.org/10.1016/j.neuron.2011.11.006

Liu, L. D., Chen, S., Hou, H., West, S. J., Faulkner, M., Laboratory, T. I. B., Economo, M. N., Li, N., & Svoboda, K. (2021). Accurate Localization of Linear Probe Electrode Arrays across Multiple Brains. *ENeuro*, *8*(6). https://doi.org/10.1523/ENEURO.0241-21.2021

Logothetis, N. K., Augath, M. A., Murayama, Y., Rauch, A., Sultan, F. F., Goense, J., Oeltermann, A., & Merkle, H. (2010). The Effects of Electrical Microstimulation on Cortical Signal Propagation. *Nature Neuroscience*, *13*(10), 1283–1293. https://doi.org/10.1038/nn.2631

Lu, S. M., Guido, W., & Sherman, S. M. (1992). Effects of membrane voltage on receptive field properties of lateral geniculate neurons in the cat: contributions of the low-threshold Ca2+ conductance. *Journal of Neurophysiology*, *68*(6), 2185–2198. https://doi.org/10.1152/JN.1992.68.6.2185

Massimini, M., Ferrarelli, F., Huber, R., Esser, S. K., Singh, H., & Tononi, G. (2005). Breakdown of Cortical Effective Connectivity During Sleep. *Science*, *309*(5744), 2228–2232. https://doi.org/10.1016/j.cogbrainres.2004.10.022

McBride, E. G., Gandhi, S. R., Kuyat, J. R., Ollerenshaw, D. R., Arkhipov, A., Koch, C., & Olsen, S. R. (2022). Influence of claustrum on cortex varies by area, layer, and cell type. *BioRxiv*, 2022.02.22.481532. https://doi.org/10.1101/2022.02.22.481532

McGinley, M. J., David, S. V., & McCormick, D. A. (2015). Cortical Membrane Potential Signature of Optimal States for Sensory Signal Detection. *Neuron*, *87*(1), 179–192. https://doi.org/10.1016/j.neuron.2015.05.038

Nestvogel, D. B., & McCormick, D. A. (2021). Visual thalamocortical mechanisms of waking state-dependent activity and alpha oscillations. *Neuron*, *0*(0). https://doi.org/10.1016/J.NEURON.2021.10.005

Oh, S. W., Harris, J. A., Ng, L., Winslow, B., Cain, N., Mihalas, S., Wang, Q., Lau, C., Kuan, L., Henry, A. M., Mortrud, M. T., Ouellette, B., Nguyen, T. N., Sorensen, S. A., Slaughterbeck, C. R., Wakeman, W., Li, Y., Feng, D., Ho, A., … Zeng, H. (2014). A mesoscale connectome of the mouse brain. *Nature*, *508*.

https://doi.org/10.1038/nature13186

Pashut, T., Magidov, D., Ben-Porat, H., Wolfus, S., Friedman, A., Perel, E., Lavidor, M., Bar-Gad, I., Yeshurun, Y., & Korngreen, A. (2014). Patch-clamp recordings of rat neurons from acute brain slices of the somatosensory cortex during magnetic stimulation. *Frontiers in Cellular Neuroscience*, *8*(JUN), 1–12. https://doi.org/10.3389/fncel.2014.00145

Patrick L. Purdon, P. ., Aaron Sampson, B. S., Kara J. Pavone, B. S., & Emery N. Brown, M.D., P. D. (2015). Clinical Electroencephalography for Anesthesiologists- Part I- Background and Basic Signatures. *Anesthesiology*, *123*(4), 937–960. https://doi.org/10.1097/ALN.0000000000000841

Pigorini, A., Sarasso, S., Proserpio, P., Szymanski, C., Arnulfo, G., Casarotto, S., Fecchio, M., Rosanova, M., Mariotti, M., Lo Russo, G., Palva, J. M., Nobili, L., & Massimini, M. (2015). Bistability breaks-off deterministic responses to intracortical stimulation during non-REM sleep. *NeuroImage*, *112*, 105–113. https://doi.org/10.1016/J.NEUROIMAGE.2015.02.056

Ragan, T., Kadiri, L. R., Umadevi Venkataraju, K., Bahlmann, K., Sutin, J., Taranda, J., Arganda-Carreras, I., Kim, Y., Seung, H. S., & Osten, P. (2012). Serial two-photon tomography: an automated method for ex-vivo mouse brain imaging HHS Public Access. *Nature Methods*, *9*(3), 255–258. https://doi.org/10.1038/nmeth.1854

Ramcharan, E. J., Gnadt, J. W., & Sherman, S. M. (2005). Higher-order thalamic relays burst more than first-order relays. *Proceedings of the National Academy of Sciences of the United States of America*, *102*(34), 12236–12241. https://doi.org/10.1073/PNAS.0502843102

Ries, C. R., & Puil, E. (1999). Mechanism of anesthesia revealed by shunting actions of isoflurane on thalamocortical neurons. *Journal of Neurophysiology*, *81*(4), 1795–1801. https://doi.org/10.1152/jn.1999.81.4.1795

Rosanova, M., Fecchio, M., Casarotto, S., Sarasso, S., Casali, A. G., Pigorini, A., Comanducci, A., Seregni, F., Devalle, G., Citerio, G., Bodart, O., Boly, M., Gosseries, O., Laureys, S., & Massimini, M. (2018). Sleep-like cortical OFF-periods disrupt causality and complexity in the brain of unresponsive wakefulness syndrome patients. *Nature Communications*, *9*, 1–10. https://doi.org/10.1038/s41467-018-06871-1

Sachidhanandam, S., Sreenivasan, V., Kyriakatos, A., Kremer, Y., & Petersen, C. C. H. (2013). Membrane potential correlates of sensory perception in mouse barrel cortex. *Nature Neuroscience 2013 16:11*, *16*(11), 1671–1677. https://doi.org/10.1038/nn.3532

Schiff, N. D., Nauvel, T., & Victor, J. D. (2014). Large-Scale Brain Dynamics in Disorders of Consciousness. *Current Opinion in Neurobiology*, *0*, 7. https://doi.org/10.1016/J.CONB.2013.10.007

Senda, D., Strong, H., Hines, D., Hines, R., & Baker, R. J. (2021). A compact 1200 V, 700 A, IGBT-based pulse generator for repetitive transcranial magnetic stimulation in vivo laboratory experiments on small animals. *Review of Scientific Instruments*, *92*(8), 084710. https://doi.org/10.1063/5.0043648

Sherman, S. M. (1996). Dual response modes in lateral geniculate neurons: Mechanisms and functions. *Visual Neuroscience*, *13*, 205–213. https://doi.org/10.1017/s0952523800007446

Siebner, H. R., Funke, K., Aberra, A. S., Antal, A., Chen, R., Classen, J., Davare, M., Di, V., Fox, P. T., Hallett, M., Karabanov, A. N., Kesselheim, J., Beck, M. M., Koch, G., Liebetanz, D., Meunier, S., Miniussi, C., Paulus, W., Peterchev, A. V, … Ugawa, Y. (2022). Transcranial magnetic stimulation of the brain: What is stimulated? – a consensus and critical position paper. *Clinical Neurophysiology*.

https://doi.org/10.1016/J.CLINPH.2022.04.022

Siegle, J. H., Jia, X., Durand, S., Gale, S., Bennett, C., Graddis, N., Heller, G., Ramirez, T. K., Choi, H., Luviano, J. A., Groblewski, P. A., Ahmed, R., Arkhipov, A., Bernard, A., Billeh, Y. N., Brown, D., Buice, M. A., Cain, N., Caldejon, S., … Koch, C. (2021). Survey of spiking in the mouse visual system reveals functional hierarchy. *Nature*, *592*(7852), 86–92. https://doi.org/10.1038/s41586-020-03171-x

Siegle, J. H., López, A. C., Patel, Y. A., Abramov, K., Ohayon, S., & Voigts, J. (2017). Open Ephys: an open-source, plugin-based platform for multichannel electrophysiology. *Journal of Neural Engineering*, *14*(4), 045003. https://doi.org/10.1088/1741-2552/AA5EEA

Sombeck, J. T., Heye, J., Kumaravelu, K., Goetz, S. M., Peterchev, A. V, Grill, W. M., Bensmaia, S., & Miller, L. E. (2022). Characterizing the short-latency evoked response to intracortical microstimulation across a multi-electrode array. *Journal of Neural Engineering*, *19*(2), 026044. https://doi.org/10.1088/1741-2552/AC63E8

Stoelzel, C. R., Bereshpolova, Y., & Swadlow, H. A. (2009). Stability of Thalamocortical Synaptic Transmission across Awake Brain States. *The Journal of Neuroscience*, *29*(21), 6851–6859. https://doi.org/10.1523/JNEUROSCI.5983-08.2009

Stringer, C., Pachitariu, M., Steinmetz, N., Reddy, C. B., Carandini, M., & Harris, K. D. (2019). Spontaneous behaviors drive multidimensional, brainwide activity. *Science*, *364*(6437). https://doi.org/10.1126/SCIENCE.AAV7893

Suzuki, M., & Larkum, M. E. (2020). General Anesthesia Decouples Cortical Pyramidal Neurons. *Cell*, *180*(4), 666-676.e13. https://doi.org/10.1016/j.cell.2020.01.024

Swadlow, H. A., & Gusev, A. G. (2001). The impact of "bursting" thalamic impulses at a neocortical synapse. *Nature Neuroscience 2001 4:4*, *4*(4), 402–408. https://doi.org/10.1038/86054

Tehovnik, E. J., Tolias, A. S., Sultan, F., Slocum, W. M., & Logothetis, N. K. (2006). Direct and indirect activation of cortical neurons by electrical microstimulation. *Journal of Neurophysiology*, *96*(2), 512–521. https://doi.org/10.1152/jn.00126.2006

Terao, Y., & Ugawa, Y. (2002). Basic mechanisms of TMS. *Journal of Clinical Neurophysiology*, *19*(4), 322–343. https://doi.org/10.1097/00004691-200208000-00006

Thibaut, A., Schiff, N., Giacino, J., Laureys, S., & Gosseries, O. (2019). Therapeutic interventions in patients with prolonged disorders of consciousness. *The Lancet Neurology*, *18*, 600–614. https://doi.org/10.1016/S1474-4422(19)30031-6

Timofeev, I., Grenier, F., & Steriade, M. (2001). Disfacilitation and active inhibition in the neocortex during the natural sleep-wake cycle: An intracellular study. *Proceedings of the National Academy of Sciences of the United States of America*, *98*(4), 1924–1929. https://doi.org/10.1073/PNAS.98.4.1924

Urbain, N., Fourcaud-Trocmé, N., Laheux, S., Salin, P. A., & Gentet, L. J. (2019). Brain-State-Dependent Modulation of Neuronal Firing and Membrane Potential Dynamics in the Somatosensory Thalamus during Natural Sleep. *Cell Reports*, *26*(6), 1443-1457.e5. https://doi.org/10.1016/J.CELREP.2019.01.038

Usami, K., Matsumoto, R., Kobayashi, K., Hitomi, T., Shimotake, A., Kikuchi, T., Matsuhashi, M., Kunieda, T., Mikuni, N., Miyamoto, S., Fukuyama, H., Takahashi, R., & Ikeda, A. (2015). Sleep modulates

cortical connectivity and excitability in humans: Direct evidence from neural activity induced by single-pulse electrical stimulation. *Human Brain Mapping*, *36*(11), 4714–4729. https://doi.org/10.1002/HBM.22948

von Bartheld, C. S., Bahney, J., & Herculano-Houzel, S. (2016). The Search for True Numbers of Neurons and Glial Cells in the Human Brain: A Review of 150 Years of Cell Counting. *J Comp Neurol*, *524*(18), 3865–3895. https://doi.org/10.1002/cne.24040

Vyazovskiy, V. V., Olcese, U., Cirelli, C., & Tononi, G. (2013). Prolonged wakefulness alters neuronal responsiveness to local electrical stimulation of the neocortex in awake rats. *Journal of Sleep Research*, *22*(3), 264. https://doi.org/10.1111/JSR.12009

Walløe, S., Pakkenberg, B., & Fabricius, K. (2014). Stereological estimation of total cell numbers in the human cerebral and cerebellar cortex. *Frontiers in Human Neuroscience*, *8*, 508. https://doi.org/10.3389/FNHUM.2014.00508

Yerkes, R. M., & Dodson, J. D. (1908). The relation of strength of stimulus to rapidity of habit-formation. *Journal of Comparative Neurology and Psychology*, *18*(5), 459–482. https://doi.org/10.1002/CNE.920180503

SUPPLEMENTAL FIGURES

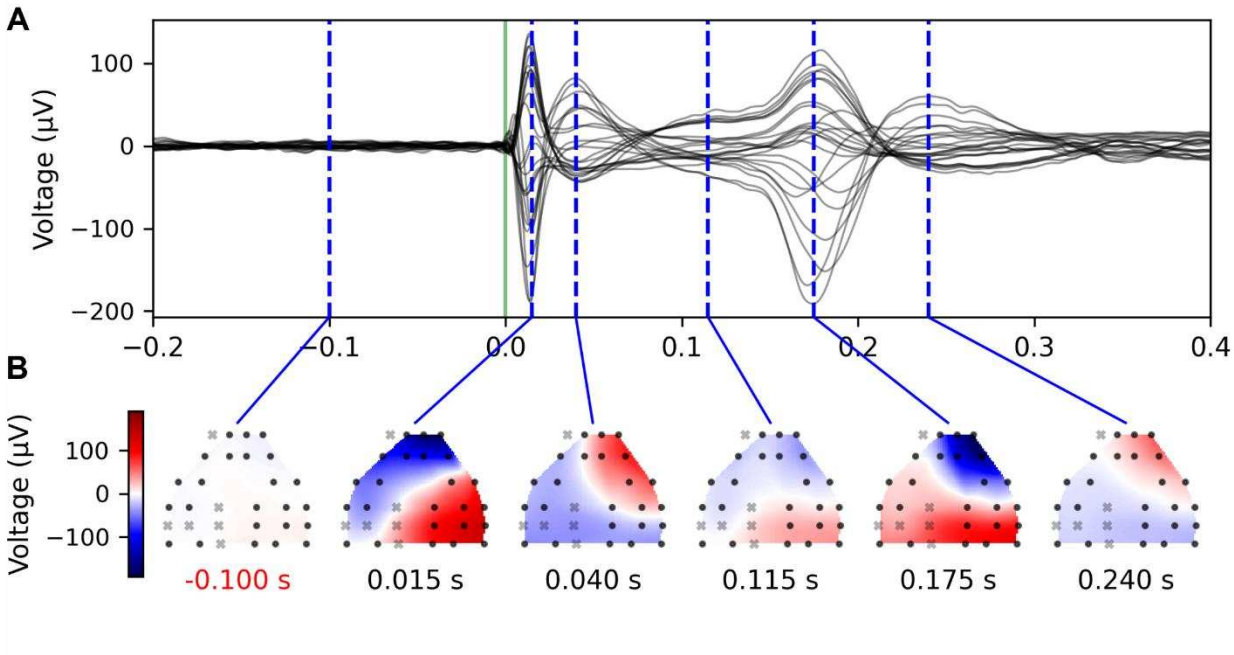

Figure S1: Spatial extent of evoked EEG responses in awake, head-fixed mice.

(A) Evoked response (-0.2 to +0.4 s around stimulus onset) from deep stimulation in MOs with all EEG electrode traces superimposed (butterfly plots). Green line marks the time of the electrical stimulus. Dashed vertical blue lines indicate the time of the spatial interpolation below. Same example as shown in Figure 1C and 1D bottom left. **(B)** The spatial interpolation of the instantaneous voltage across the surface of the mouse brain sampled by the EEG electrodes. Black circles and gray x-marks represent electrodes that did and did not pass a quality control step, respectively. The white band running across cortex represents the transition between the two polarities of the EEG signals.

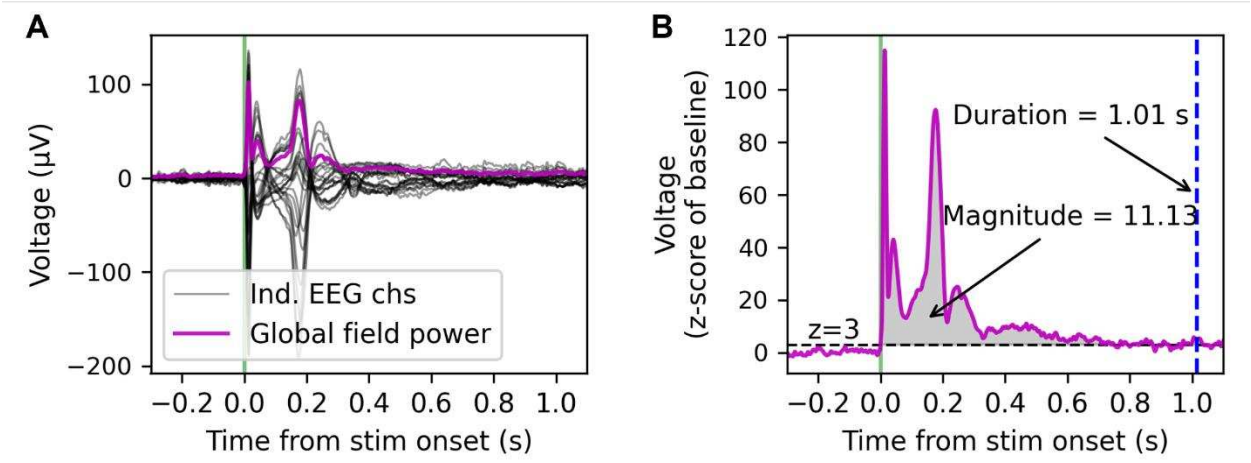

Figure S2: Demonstration of duration and magnitude calculation for evoked responses.

(A) Evoked response (-0.3 to +1.1 s around stimulus onset) from deep stimulation in MOs with all EEG electrode traces superimposed (black lines). The magenta line represents the global field power, the standard deviation of voltage values across all electrodes at each time sample. Green line marks the time of the electrical stimulus. Same example as shown in Figure 1C and 1D bottom left. **(B)** The global field power (baseline z-score; -0.3 to +1.1 s around stimulus onset) from panel A. The duration of the evoked response is measured by the length of time the global field power remains above a threshold of three standard deviations above the baseline mean (z=3, represented by the horizontal, black, dashed line) in the response window from stimulus onset to +2 s after. The duration of this example is 1.01 s, represented by the vertical, dashed, blue line. The magnitude of the evoked response is measured by the area under the curve of the z-scored global field power above the threshold (z=3) in the response window from stimulus onset to +2 s after. The magnitude of this example is 11.13 (normalized units) and represented by the gray shaded region.

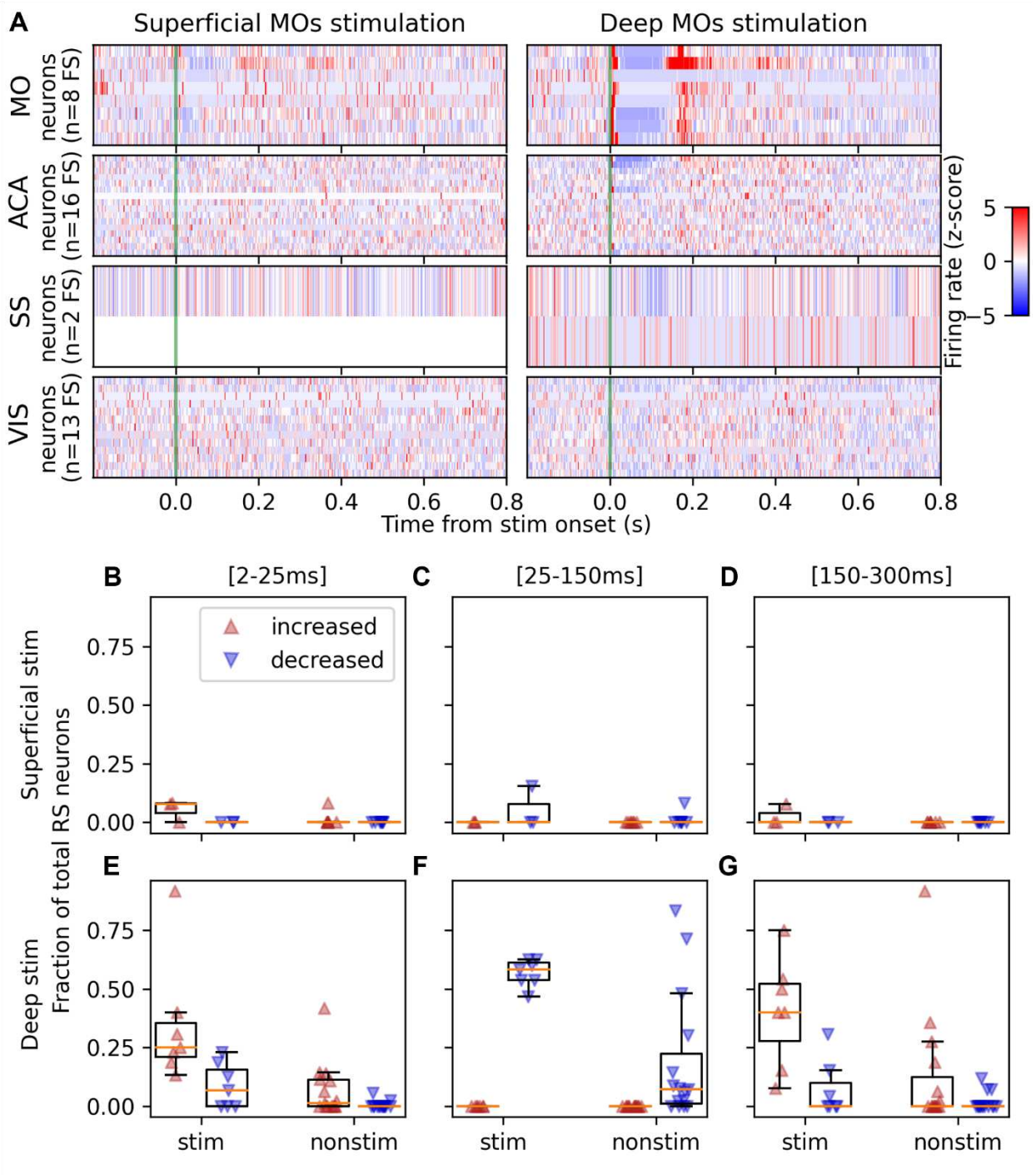

Figure S3: The fraction of the FS neuron population that is significantly modulated depends on the layer of stimulation.

(A) The fraction of FS neurons that exhibit a significantly increased (red upward triangle) or decreased (blue downward triangle) response in the first 25 ms for mice that received superficial stimulation. **(B)** The fraction of FS neurons that exhibit a significantly increased or decreased response 25-150 ms following the stimulus. **(C)** The fraction of FS neurons that exhibit a significantly increased or decreased response 150-300 ms following the stimulus. **(D-F)** Same as panels A-C but for subjects that received deep stimulation. Data from experiments with

superficial cortical stimulation (**top**, 156 FS neurons from stimulated cortex and 507 FS neurons from non-stimulated cortical regions in N=7 mice) and with deep cortical stimulation (**bottom**, 309 FS neurons from stimulated cortex and 1,206 FS neurons from non-stimulated cortical regions in N=15 mice). Boxplots show median (orange line), 25th, and 75th percentiles; whiskers extend from the box by 1.5x the IQR.

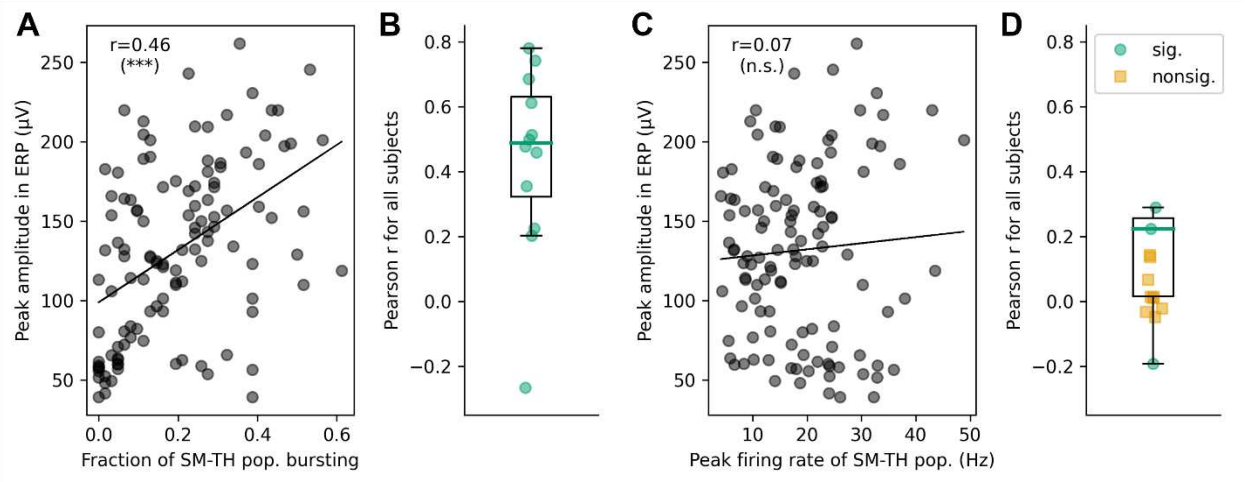

Figure S4: The amplitude of the second, late component in the ERP is correlated with the SM-TH bursting, but not the population firing rate.

(A) The Pearson correlation between the peak amplitude of the second, late component in the ERP and the fraction of the SM-TH that bursts on a trial-by-trial basis for one example mouse (same subject as in Figure 1D bottom left). **(B)** The correlation value (Pearson r) for the comparison in panel **A** for all subjects with deep stimulation (N=12 mice), green circles represent subjects with a significant correlation ($p<0.05$) and yellow squares represent subjects with a non-significant correlation. **(C)** The Pearson correlation between the peak amplitude of the second, late component in the ERP and the peak SM-TH population firing rate on a trial-by-trial basis for one example mouse (as in panel **A**). **(D)** The correlation value (Pearson r) for the comparison in panel **C** for all subjects with deep stimulation (N=12 mice), represented as in panel **B**. Boxplots show median (green line), 25th, and 75th percentiles; whiskers extend from the box by 1.5x the IQR. * $p < 0.05$, ** $p < 0.01$, *** $p < 0.001$.